Journal of Inflammation Research Dovepress

Open Access Full Text Article ORIGINAL RESEARCH

Astragalus Polysaccharide Mitigates Rhabdomyolysis-Induced Acute Kidney Injury via Inhibition of M1 Macrophage Polarization and the cGAS-STING Pathway

Chuanchuan Sun[1,2], Xinhai Zhao[1], Xianghong Wang[3], Yeye Yu[1], Heng Shi[4], Jun Tang[5], Shengyun Sun[1], Shiping Zhu[1]

[1]Department of Traditional Chinese Medicine, The First Affiliated Hospital of Jinan University, Guangzhou, People's Republic of China; [2]Department of Nephrology, The First Affiliated Hospital of Jinan University, Guangzhou, People's Republic of China; [3]Department of Endocrinology and Metabolism, Zhuhai People's Hospital (Zhuhai Clinical Medical College of Jinan University), Zhuhai, People's Republic of China; [4]Department of Gastroenterology, The Central Hospital of Shaoyang, Shaoyang, People's Republic of China; [5]The Fifth Affiliated Hospital of Zunyi Medical University, Zhuhai(Zhuhai Sixth People's Hospital), Zhuhai, People's Republic of China

Correspondence: Shengyun Sun; Shiping Zhu, Department of Traditional Chinese Medicine, The First Affiliated Hospital of Jinan University, No. 613 Huangpu Avenue West, Tianhe District, Guangzhou, Guangdong Province, 510630, People's Republic of China, Email shengyunsun2020@163.com; zhushiping@jnu.edu.cn

Purpose: This study aimed to examine the impact of APS on acute kidney injury induced by rhabdomyolysis (RIAKI), exploring its association with macrophage M1 polarization and elucidating the underlying mechanisms.

Methods: C57BL/6J mice were randomly assigned to one of three groups: a normal control group, a RIAKI model group, and an APS treatment group. Techniques such as flow cytometry and immunofluorescence were employed to demonstrate that APS can inhibit the transition of renal macrophages to the M1 phenotype in RIAKI. Furthermore, the raw264.7 macrophage cell line was chosen and induced into the M1 phenotype to further examine the impact of APS on this model and elucidate the underlying mechanism.

Results: Administration of APS led to a significant decrease in UREA levels by 25.2% and CREA levels by 60.9% within the model group. Also, APS exhibited an inhibitory effect on the infiltration of M1 macrophages and the cGAS-STING pathway in kidneys within the RIAKI, subsequently leading to decreased serum concentrations of IL-1β, IL-6 and TNF-α by 44.5%, 12.9%, and 10.3%, respectively, consistent with the results of in vitro experiments. Furthermore, APS exhibited an anti-apoptotic effect on MPC5 cells when co-cultured with M1 macrophages.

Conclusion: Astragalus polysaccharide (APS) potentially mitigated rhabdomyolysis-induced renal damage by impeding the M1 polarization of macrophages. This inherent mechanism might involve the suppression of the cGAS-STING pathway activation within macrophages. Furthermore, APS could endow protective effects on podocytes through the inhibition of apoptosis.

Keywords: astragalus polysaccharide, macrophages, rhabdomyolysis-induced acute kidney injury, cGAS-STING pathway

Introduction

Rhabdomyolysis is a clinical syndrome characterized by muscle necrosis and myoglobinuria that can occur in the setting of military activities, natural disasters, strenuous exercise, trauma, infections, genetic defects, heavy alcohol use, and drug use et al. Following muscle injury, muscle cell constituents such as myoglobin, creatine kinase, lactate dehydrogenase, potassium, and sodium leaked into the extracellular fluid, which can lead to clinical problems such as acute kidney injury (AKI), heart failure, and electrolyte disturbances. Rhabdomyolysis-induced acute kidney injury (RIAKI) is a major cause of AKI, accounting for up to 10% of all cases of AKI,[1,2] and has a mortality rate ranging from 10% to 50%.[3] Patients with RIAKI often require renal replacement therapy. A single episode of RIAKI can lead to a slowly progressive decline in renal function and ultrastructural changes in the kidney, which can progress to renal fibrosis and chronic kidney disease (CKD).[4–6]

Received: 5 September 2024
Accepted: 5 December 2024
Published: 23 December 2024

The early management of RIAKI primarily entails prompt and robust fluid resuscitation, urinary alkalinization. This approach also necessitates the maintenance of acid-base and electrolyte balance, promotion of diuresis, implementation of antioxidant therapies, and when indicated, renal replacement therapy.[7] However, the formulation of specific treatment plans must be individualized based on patient-specific factors such as age, gender, and comorbid conditions, which poses significant challenges in clinical practice. Furthermore, there is a notable absence of personalized therapeutic regimens that target specific genetic profiles or molecular pathways. Currently, there is no effective treatment for RIAKI.

Macrophages play a crucial role in maintaining tissue homeostasis and immune defense.[8] Dysregulated macrophage polarization is involved in the development and progression of kidney diseases. In the RIAKI model, a phenotypic switch in macrophages had been observed,[5,9–11] accompanied by activation of the STING pathway,[6] which further exacerbated renal injury and fibrosis. Immunotherapy targeting represents a burgeoning area of research in the treatment of RIAKI.[12] Strategies aimed at inhibiting the M1 anti-inflammatory phenotype of macrophages, promoting transition to the M2 phenotype, and depleting macrophages have been shown to mitigate renal injury and fibrosis,[5,9,10] thereby enhancing long-term renal outcomes. Consequently, modulating the phenotype of renal macrophages is postulated to represent a novel direction for future therapeutic interventions in the management of RIAKI.

APS is a polysaccharide extracted from Astragalus membranaceus, which has a wide range of pharmacological activities. Previous studies have demonstrated that APS exhibited activities such as anti-inflammatory, antioxidant, immunomodulatory, anti-aging and anti-tumor effects.[13] However, whether APS can modulate macrophage function and cGAS-STING pathway in RIAKI remains unclear. In our study, we established an acute kidney injury model induced by rhabdomyolysis and employed APS for pretreatment. We found that the pretreatment with APS effectively mitigated macrophage infiltration in the kidneys lured by rhabdomyolysis, revealing a potential protective effect of APS against AKI. These findings provide indispensable theoretical foundation for the clinical application of APS in the management of related disorders.

Materials and Methods

Reagents and Antibodies

Foetal bovine serum (FBS), Dulbecco's Modified Eagle Medium (DMEM) (High Glucose) and RPMI 1640 medium were purchased from Gibco. The following antibodies were employed in this experiment: iNOS antibody (22226-1-AP, Proteintech), anti-TMEM173/STING (19851-1-AP, Proteintech), anti-cGAS (55482–1, SAB), anti-cGAS (29958-1-AP, Proteintech), anti-IRF3 (ab238521, Abcam), anti-Tubulin beta (AF7011, Affinity), anti-CD16/32 (14016182, Invitrogen), eFluor 450 CD86 antibody (2546909, Invitrogen), PE CD206 antibody (141706, BioLegend), PerCP-eFluor 710 IL-1β antibody (2492131, Invitrogen), FITC IL-6 antibody (2416199, Invitrogen), PE/Cyanine7 TNF-α antibody (506324, BioLegend). IL-1β, IL-6, TNF-α and MYO enzyme-linked immunosorbent assay (ELISA) kits were procured from MEIMIAN.

Animals and Rhabdomyolysis-Induced AKI Model

This work was authorized by Jinan University's Ethics Committee. The care and use of laboratory animals was governed by defined rules in accordance with the People's Republic of China GBT 42011–2022 standards for laboratory animal guidelines for ethical review of animal welfare, which were followed in all animal experiments. Male C57BL/6J mice, aged 6–8 weeks (20–23g), were purchased from Guangdong Medical Laboratory Animal Center and kept in a temperature-controlled, pathogen-free environment, following defined rules for the care and use of laboratory animals, including a 12-hour light/dark cycle. Water and food were freely available to animals. The animals were randomly assigned to three groups: APS (A860847, Macklin, Shanghai, China) pretreatment group, RIAKI model group, and normal control group. Each group consisted of 8 mice. To induce rhabdomyolysis, based on relevant literature and the body weight of the mice,[14,15] we conducted the model according to the following steps: mice were anesthetized with 2% isoflurane (R510-22-10, Ryward RWD, Shenzhen, China), and then underwent intramuscular injections of either saline as

a control or 8 mL of 50% glycerol (HY-B1659, Macklin, Shanghai, China) diluted with sterile water per kg body weight into both of their thigh muscle. Proper pain relief measures such as 2% isoflurane (R510-22-10, Ryward RWD, Shenzhen, China) were included to minimize animal discomfort during the procedure. For seven consecutive days prior to rhabdomyolysis induction, the APS pretreatment group received 100 mg of APS per kg of body weight via gavage. Two hours after the seventh day, 8.0 mL/kg of 50% glycerol was injected intramuscularly. Mice were euthanized with CO_2 inhalation 24 hours after the administration of drugs to minimize suffering and in accordance with the approved ethical guidelines. Following the experiment, all mice were sacrificed and their blood and kidneys were collected.

Kidney Coefficient

All mice were weighed using an electronic balance before sacrifice, and both kidneys of each mouse were removed for weight measurement after sacrifice. Finally, the ratio of the weight of each mouse kidney to its body weight was calculated to obtain the kidney coefficient.

Renal Function Detection

Using the proper kits and operating manual guidance, automatic biochemistry analyzer (MINDRAY, BS-360E, Shenzhen, China) should be used to evaluate creatinine and urea nitrogen.

Enzyme Linked Immunosorbent Assay (ELISA)

After collecting mouse blood in sterile tubes and leaving them at room temperature for 1–2 hours to thoroughly coagulate, centrifuged them at 4°C 3000rpm for 30min, obtained the supernatant scrupulously. The ELISA kits (MEIMIAN, China) were used to measure the levels of cytokines (IL-1β, IL-6, TNF-α) and MYO in accordance with the manufacturer's instructions.

Flow Cytometry of the Kidneys

Following the kidney's surgical removal, the kidneys were minced with ophthalmic scissors, homogenized and digested with collagenase (17104019; Thermo Fisher Scientific, USA) for 30min, 37°C, centrifuged for 5 minutes at 1500 rpm, and erythrocyte lysate (Beyotime, China) was employed to lyse red blood cells and then filtered through a 70μm filter to a 15 mL centrifuge tube.[16] Once centrifuged and counted, the mixture was resuspended with RPMI 1640 medium (C11875500BT, Gibco, Grand Island, USA), filtered and spread to a 24-well plate at 2.5×10^5 per well, with cell stimulation solution (ION[S1672, Beyotime, China] +PMA[P8139, Sigma-Aldrich, USA]+ Golgi-Plug [555029, BD, USA]), and then placed in a CO_2 cell culture incubator for 4–6 hours for stimulation. Once accomplished, the cells were collected, washed, following by CD16/32 blocking Fc fragment. Cells were first labeled on their surface antibodies, then fixed and perforated for intracellular staining. Cells were analyzed using the Cytek Northern Lights (Cytek Biosciences, USA). The FlowJo software was deployed to conduct the flow cytometry analysis.

Histopathological Assessment

Kidneys that were collected were embedded in paraffin, preserved in 4% paraformaldehyde fix solution (4% PFA Fix Solution) for 24 hours, embedded in paraffin, cut into 5 μm thickslides, and stained with hematoxylin and eosin (H&E), Periodic acid Schiff (PAS), or Masson to analyze the histology of samples. Tubular damage was characterized by necrotic lysis, tubular dilation, cast formation, and the sloughing of cellular debris into the tubular lumen. The severity of renal tubule injury was graded based on the percentage of affected tubules: 0 for no damage, 1 for <25% involvement, 2 for 25–50% involvement, 3 for 50–75% involvement, and 4 for >75% involvement.[17] The degree of fibrosis was measured by Masson staining. Analysis using immunohistochemistry was done to gauge the kidney's protein expression. The slides were scanned using a fully automatic slide scanning microscope (TissueGnostics, Austria).

Immunofluorescence Staining

Kidney sections or cells were fixed with 4% paraformaldehyde and subsequently blocked with 3% bovine serum albumin (BSA) for 30 minutes. The primary antibodies, which constituted a mixture of two different first primary antibodies

intended for double staining, were then applied and allowed to incubate overnight at a temperature of 4°C. Then the sections were incubated with CY3-labelled goat anti-rabbit IgG (GB21303, Servicebio, China) and Alexa Fluor 488-labelled goat anti-rabbit IgG (GB25303, Servicebio, China) for a period of 50 minutes at room temperature under conditions of darkness. The cell nuclei were subsequently counterstained with DAPI. The slides were scanned with TissueGnostics.

Cell Culture and Treatment

Raw264.7 cells, a mouse leukemic monocyte/macrophage cell line, were obtained from the American Type Culture Collection (ATCC, Manassas, VA, USA), which was cultured in DMEM media supplemented with 10% fetal bovine serum and 1% penicillin-streptomycin and were incubated at 37 °C maintaining 5% CO2 in a cell incubator. To simulate M1 polarization in raw 264.7 cells, LPS (100ng/mL, Biosharp, China)+IFN-γ (20 ng/mL, Peprotech, USA) were utilized. Cells were distributed into four groups: normal control, M1, M1+50μg/mL APS, M1+100μg/mL APS. Raw264.7 cells kept in standard medium were utilized as a control. Cells of the M1 macrophages were cultured in DMEM medium containing 100ng/mL LPS and 20ng/mL IFN-γ for 24 h. Then, M1 macrophages were incubated for 24 hours with 50μg/mL and 100μg/mL of APS, respectively.

RNA Extraction and Quantitative Real-Time PCR (RT-qPCR)

Total RNA isolation was performed using Total RNA Extraction Kit (RE-03113, Foregene, China) in accordance with the manufacturer's instructions, measured the concentration with NanoDrop 2000 (Thermo Scientific, USA) and diluted into equal volumes with diethylpyrocarbonate (DEPC) water (Beyotime, Shanghai, China). PrimeScript RT reagent Kit with gDNA Eraser (RR047A, TaKaRa, Japan) were adopted to remove gDNA and reverse transcribe them to cDNA pursuant to the directions. TB Green® Premix Ex Taq™ II (Tli RNaseH Plus) (RR820A, TaKaRa, Japan) were exploited for qPCR. The data were adjusted to match the GAPDH expression. The normalization and analysis of the data were done applying to the ΔΔCt method. The primers were synthesized by Guangzhou Ige Biotechnology Ltd. Primer sequences are shown in Table 1.

Protein Extraction and Western Blotting

In six-well plates, 1×10^6 of raw264.7 cells were seeded per well. The cells were then wall-adhered, subjected to LPS, IFN-γ induction, and APS treatment for 48 hours, washed the cells with PBS and then added lysis buffer (RIPA buffer) supplemented with protease and phosphatase inhibitors to extraction total cell proteins. The protein concentrations were measured using the BCA protein kit (BB-3401, Bestbio, China). Using 7.5% or 10% SDS-PAGE gels (Shanghai Epizyme Biomedical Technology Co., Ltd, China), the denatured protein was separated and then placed onto PVDF membrane (Millipore, USA). The PVDF membrane was blocked with 5% nonfat milk for one hour, and incubated at 4 °C overnight with primary antibodies. Following TBST washing and a 2-hour room temperature incubation period with secondary

Table 1 Primers Used in the Article

Gene Name	Forward	Reverse
GAPDH	AGGTCGGTGTGAACGGATTTG	TGTAGACCATGTAGTTGAGGTCA
CD86	GAGCACTATTTGGGCACAGAGAAAC	TGAAGTCGTAGAGTCCAGTTGTTCC
iNOS	CTCTAGTGAAGCAAAGCCCAAC	CCTCACATACTGTGGACGGG
Havcr1(KIM1)	ACATATCGTGGAATCACAACGAC	ACAAGCAGAAGATGGGCATTG
Lcn2(NGAL)	GGGAAATATGCACAGGTATCCTC	CATGGCGAACTGGTTGTAGTC
cGAS	TGCTGGACAAATTGAGATTGAAACG	CCACACCTTTGAACTCCGACTC
Sting1	GGTCACCGCTCCAAATATGTAG	CAGTAGTCCAAGTTCGTGCGA
IRF3	CTGACAATAGCAAGGACCCTTA	AGGCCATCAAATAACTTCGGTA
IL-1β	TCGCAGCAGCACATCAACAAG	TCCACGGGAAAGACACAGGTAG
IL-6	CTCCCAACAGACCTGTCTATAC	CCATTGCACAACTCTTTTCTCA
TNF-α	CTTCTCATTCCTGCTTGTGGC	ACTGATGAGAGGGAGGCCATT

antibody, the membrane was exposed using the Gel Imaging and Analysis System (Sage Creation, China). A housekeeping protein was HSP90 or β-Tubulin.

Measuring Intracellular ROS Levels

We used the Beyotime ROS Assay Kit (S0033S, Shanghai, China) in accordance with the instructions to assess the amounts of intracellular reactive oxygen species. Briefly, the cell culture medium from the six-well plates was discarded and washed three times with free DMEM. Subsequently, the cells were subjected to a 30-minute incubation at 37°C with 10μmol/L of DCFH-DA in 1 mL of free DMEM. They were then rinsed three times with PBS and examined under a fluorescence microscope (excitation wavelength was set at 485 nm, emission was collected at 520 nm) (Leica, German).

Detection of Mitochondrial Membrane Potential

As instructed, we used the Mitochondrial Membrane Potential Assay Kit with JC-1 to evaluate the mitochondrial membrane potential. Removed the culture medium from a six-well plate and washed the cells once with PBS and added 1mL of cell culture medium. Then, added 1mL of JC-1 staining working solution and mix thoroughly. Incubated at 37°C in the cell culture incubator for 20 minutes. Additionally, aspirated the supernatant and flushed the cells twice with JC-1 staining buffer (1X). The cells were checked under a fluorescence microscope (Excitation light can be set to 490 nm and emission light to 530 nm for JC-1 monomer detection; excitation light can be set to 525 nm and emission light to 590 nm for JC-1 polymer detection) (Leica, German).

Establishment of a Co-Culture System

We used transwell chambers to establish a co-culture system of M1 macrophages stimulated by LPS and IFN-γ in the top chamber with the mouse podocyte cell-line MPC-5 in the lower chamber. There were three distinct groups, control, co-culture, and APS treatment. In the control group, the upper chamber was filled with cell-free media while in the APS treatment group the lower chamber of the APS was supplemented with 100 μg/mL of APS. The co-culture procedure lasted 48 hours.

Annexin V Assessment for Apoptosis

The Annexin V-FITC/PI Apoptosis Detection Kit (MA0220, Meilunbio) was deployed to track down cell apoptosis. Concisely, following the aforementioned co-culture system, cell mass precipitation was collected and washed with ice-cold 1× PBS. Afterwards, cells were fixed in binding buffer and 5 μL Annexin V-FITC for 15 minutes at room temperature. Following the addition of the PI regent (5 μL), flow cytometry was exploited to scrutinize the cells.

CCK-8 Assay

Raw264.7 cells were planted at a density of 8000 cells/well into 96-well plates. Following cell attachment, APS was applied to cells at a range of concentrations for 24 hours or 48 hours. CCK8 solution (10 μL/well) was added, and incubated for 2 hour. Thereafter, the OD values (450 nm) were measured using Varioskan LUX (Thermo Fisher Scientific). The data normalized to the untreated control and presented as "% Inhibition" applying to the ensuing formula: $(OD_A - OD_B)/(OD_C - OD_B)$ 100%, which ascertain IC_{50} values.

Statistical Analysis

Data were presented as means ± SD or means ± S.E.M. All experiments are repeated at least three times. GraphPad Prism 9.5 software is utilized to analyze data that is typically distributed and analyzed using one-way ANOVA or Student's *t*-test. Statistical significance is achieved when $p < 0.05$.

Results

Astragalus Polysaccharides Alleviated Acute Kidney Injury Induced by Rhabdomyolysis

We initially confirmed the renoprotective effect of APS against renal injury mingled with rhabdomyolysis in C57/BL6J mice. The procedure for in vivo induction of rhabdomyolysis is delineated in Figure 1. Upon completion of the experiment, we euthanized the mice and collected renal specimens, which exhibited a waxen, contracted appearance indicative of ischemia (Figure 2a), along with decreased overall body weight of the mice (Figure 2b), while increased kidney weight (Figure 2c) and kidney index (Figure 2d). The administration of APS significantly lowered serum levels of MYO, UREA and CREA by 8.8%, 25.2%, 60.9%, concomitantly enhancing the mRNA expression of kidney injury molecule-1 (KIM-1) and neutrophil gelatinase-associated lipocalin (NGAL), as illustrated in Figure 2e–h, hinting muscle dissolution and renal function impairment.

Histopathological examination of the model group stained with hematoxylin and eosin (H&E) revealed glomerular and tubular injuries (Figure 2i, and m), characterized by enlarged Bowman's capsule and intratubular cast formation. Periodic acid-Schiff (PAS) staining showed glycogen deposition (Figure 2j and n), while Masson staining revealed fibrous component accumulation (Figure 2k and o). These findings concealed that APS pretreatment exerts protective effects against RIAKI and glycerol-induced muscle damage.

APS Suppressed M1 Macrophage Polarization and Inflammatory Cytokine Production in RIAKI

Macrophages play a crucial role in the pathogenesis of RIAKI. After sacrificing the mice, we harvested kidney samples and used F4/80 to identify resident renal macrophages and CD86 to label M1 macrophages. Also, we measured the inflammatory factors IL-1β, IL-6, and TNF-α secreted by M1 macrophages and applied flow cytometry to differentiate these cell populations (Figure 3a). We observed a significant increase in CD86-positive macrophages in the model group compared to the control group, which was statistically significant. Correspondingly, the inflammatory cytokines IL-1β, IL-6, and TNF-α were elevated in the model group. In the APS-treated group, both CD86-positive macrophages and inflammatory cytokines were reduced (Figure 3b–e). Additionally, immunofluorescence co-localization revealed an increase in renal macrophages in the model group, particularly CD86-positive macrophages (Figure 3f), which aligned with the results of renal immunohistochemistry and renal tissue qPCR, revealing elevated levels of renal M1 macrophage markers CD86 and iNOS in the model group (with statistical significance compared to the control group), conversely reduced in the APS-treated group (with statistical significance compared to the model group) (Figure 3g–j). Renal tissue qPCR and ELISA assays delivered that the levels of IL-1β, IL-6, and TNF-α in the blood were consistent with the alterations in inflammatory cytokine levels in the kidneys (Figure 3k–n). In brief, APS treatment significantly reduced IL-1β, IL-6, and TNF-α serum levels in the model group by 44.5%, 12.9%, and 10.3%, respectively. In other words, APS can ameliorate rhabdomyolysis-induced kidney damage by extinguishing M1 macrophage polarization.

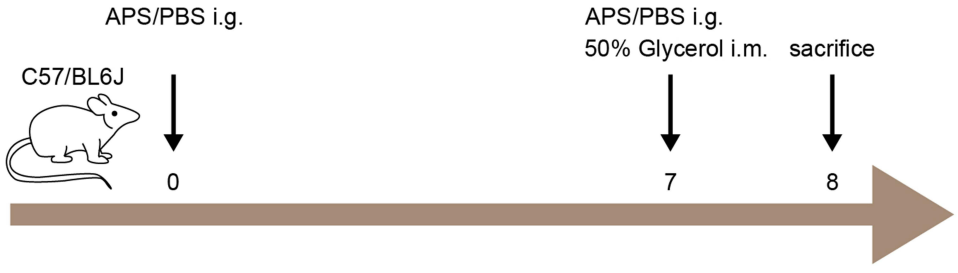

Figure 1 Experimental approach for the induction of rhabdomyolysis-induced acute kidney injury in mice. 50% glycerol was administered intramuscularly into the hind limbs of mice at a dose of 8 mL/kg. Mice with saline injections served as controls. To appraise the protective effect of APS, 100mg/kg body weight of APS or phosphate-buffered saline (PBS) was administered by oral gavage for 7 consecutive days prior to intramuscular injection of glycerol. Mice were euthanized for blood and kidney samples within 24 hours of receiving a glycerol injection.

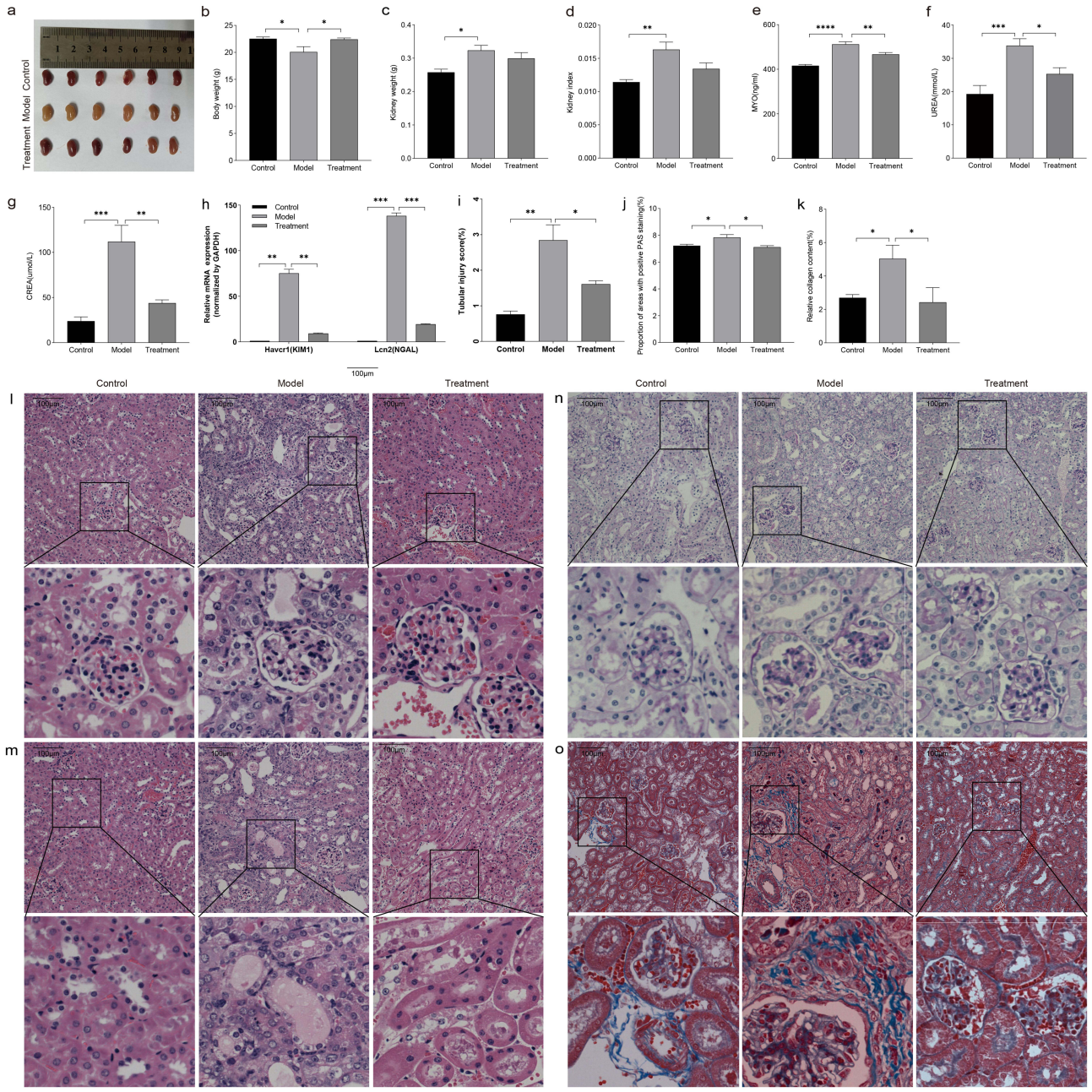

Figure 2 Astragalus polysaccharides mitigated rhabdomyolysis-induced acute kidney injury. (**a**) Gross appearance of mouse kidneys: We observed that the kidneys of mice in the model group were enlarged and exhibited an ischemic appearance, while the kidneys in the pretreatment group were dark red. (**b–d**) Body weight, kidney weight and kidney index changes in mice in the control group, model group, and treatment group. The body weight of mice in the model group decreased, while that of mice in the pretreatment group increased. The kidney weight and kidney index of mice in the model group elevated, which may be related to inflammation, hyperperfusion, and edema in the kidneys after rhabdomyolysis. However, the aforementioned two indicators lowered in the treatment group, demonstrating the renoprotective influence of APS. (**e–g**) Changes in blood serum MYO, UREA and CREA in mice: The MYO, UREA, CREA level was markedly elevated in the model group. Together with the renal function, renal pathology, and myoglobin parameters, this indicated successful modeling. (**h**) The qPCR analysis of mRNA expression levels of Havcr1(KIM1) and Lcn2(NGAL) of kidneys. (**i**) Pathological scoring of renal tubular injury. Statistical significance was determined by two-way ANOVA followed by Tukey's post hoc test. (**j**) Quantification of PAS-positive staining area. k. Quantification of Masson staining and collagen fiber-positive area. (**l**) H&E staining of mouse kidneys showing glomeruli and localized enlargement: the glomerular capsular area was enlarged in the model group. (**m**) H&E staining of mouse kidneys revealing renal tubules and enlargement: intratubular casts were observed in the lumen of renal tubules. (**n** and **o**) PAS and Masson staining of mice and enlargement images.*p<0.05; **p<0.01, ***; p<0.001; ****p<0.0001; Control: normal control group; Model: rhabdomyolysis-induced acute kidney injury model; Treatment: pretreatment with APS. Magnification: 20x, scale bar: 100μm.

Target Screening of RIAKI and Astragalus Polysaccharide

To identify the targets of RIAKI and Astragalus polysaccharide, we utilized "rhabdomyolysis induced acute kidney injury" as the search term. We conducted searches in three databases, Genecards (https://www.genecards.org),[18] OMIM (https://www.omim.org),[19] and TDD (https://db.idrblab.net/ttd),[20] selecting human species-specific target genes. A total

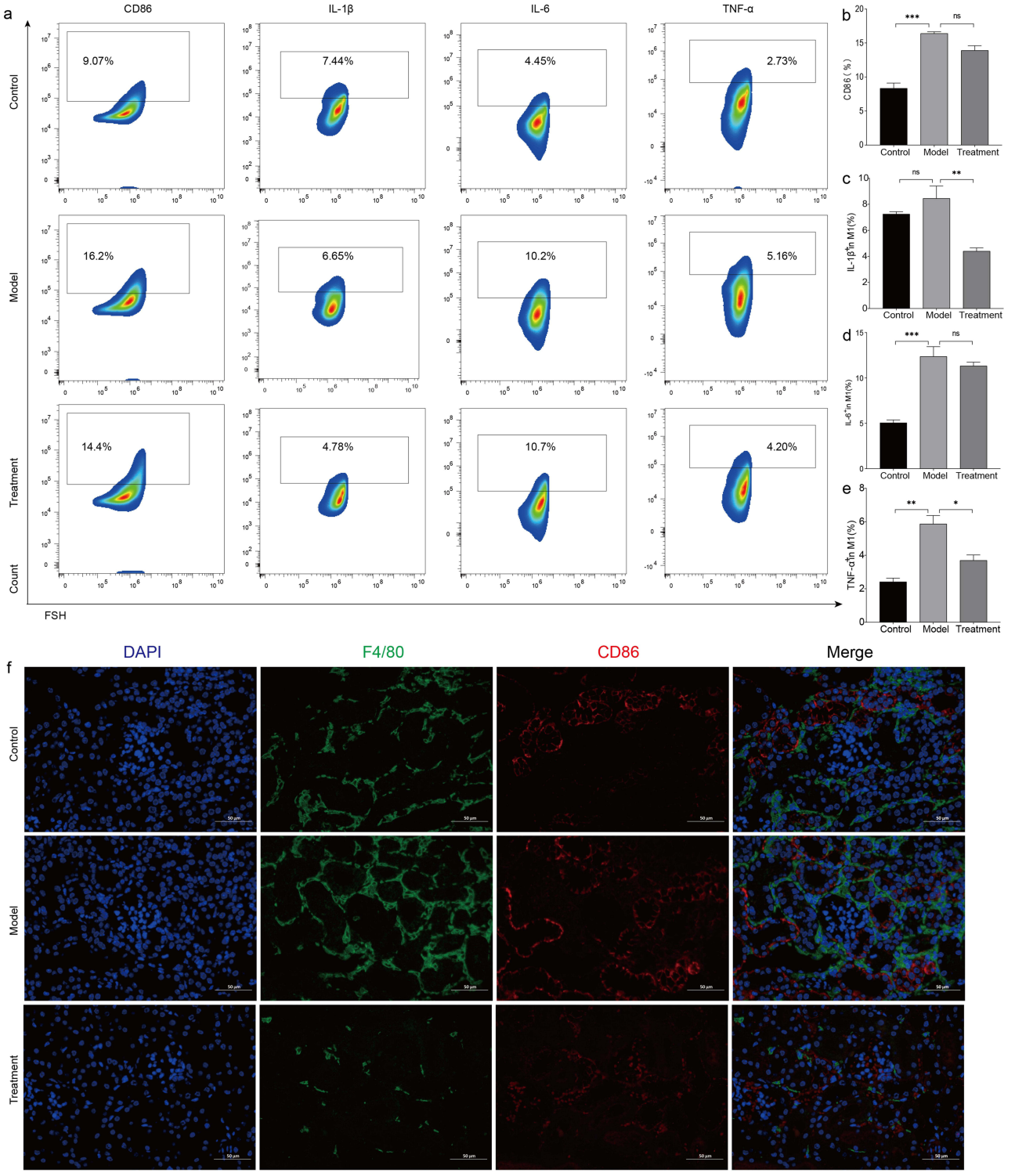

Figure 3 Continued.

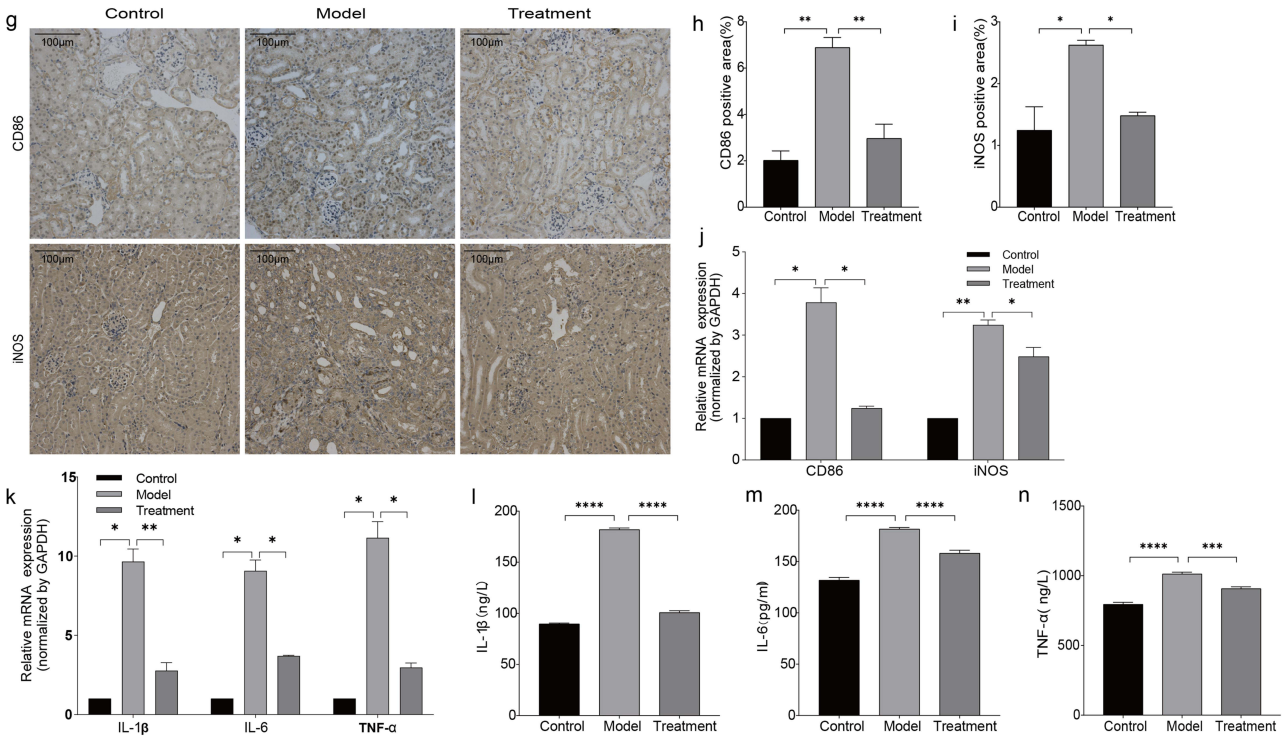

Figure 3 APS suppressed M1 macrophage polarization and inflammatory cytokine production in RIAKI. (**a**) Flow cytometry of mouse kidneys, with specific labeling of M1 macrophage marker CD86 and its inflammatory factors IL-1β, IL-6, and TNF-α. (**b–e**) Flow cytometry plots showing the percentage of CD86, IL-1β, IL-6, and TNF-α-positive cells in mouse kidneys. The model group exhibited elevated levels of CD86 and cytokines in kidneys, while the pretreatment group showed a significant reduction in these signs. (**f**) Immunofluorescence colocalization images of F4/80 (M0) and CD86 (M1) in kidneys(Magnification: 40x, scale bar: 100μm). We noticed marked increase in M1 macrophages in the kidneys of the model group and significant reduction in the treatment group. (**g**) Immunohistochemical staining of mouse kidneys for M1 macrophage markers CD86 and iNOS(Magnification: 20x, scale bar: 100μm.). (**h–i**) Quantification of CD86 and iNOS expression by immunohistochemistry (IHC) in mouse kidneys. The analysis demonstrated a considerable escalation in M1 macrophage markers in the model group, which was drastically depleted in the treatment group. (**j**) The qPCR analysis of mRNA expression levels of CD86 and iNOS of kidneys. (**k**) mRNA expression levels of IL-1β, IL-6, and TNF-α of kidneys. (**l–n**) Quantification of serum inflammatory cytokines IL-1β, IL-6, and TNF-α in mice. The model group exhibited statistically substantial elevations in serum IL-1β, IL-6, and TNF-α levels, while the treatment group displayed falls in these parameters.

Note: *p<0.05; **p<0.01; ***p<0.001; ****p<0.0001.

Abbreviation: ns, not statistically significant.

of 1142 target genes were obtained (Figure 4a). Subsequently, we employed the TCMSP platform (https://old.tcmsp-e.com/tcmsp.php)[21] with screening criteria of oral bioavailability (OB) ≥30% and drug-likeness ≥0.18 based on pharmacokinetic parameters to obtain core drug activity and targets. The obtained target genes were normalized using the UniProt database (https://www.uniprot.org/),[22] resulting in 207 target genes (Figure 4b). The obtained target genes of RIAKI and Astragalus were intersected using an online tool (https://bioinfogp.cnb.csic.es/tools/venny) to obtain 41 intersection target genes (Figure 4c). Subsequently, we retrieved the TSV format file of protein–protein interaction (PPI) relationships from the STRING database (https://cn.string-db.org),[23] removing free genes, and imported it into Cytoscape 3.9.1 for visual network topology analysis (Figure 4d). We dispatched the 41 intersecting genes to the DAVID database[24] for Gene Ontology (GO) and Kyoto Encyclopedia of Genes and Genomes (KEGG) pathway analysis. The results of the analysis were visualized using an online tool available at http://www.bioinformatics.com.cn/(Figure 4g and h). We found that the intersection mainly focused on the genes TNF, IL-6, and IL-1B. Since the inflammatory factors expressed by these genes are mainly activated by M1 macrophages, consistent with our previous studies, Astragalus polysaccharide may primarily act to inhibit M1 polarization of macrophages to alleviate rhabdomyolysis-induced renal injury. We identified IRF3 and TBK1 among the target genes of RIAKI, as IRF3 is downstream of Sting1. Focusing on the cGAS-STING pathway, through the STRING protein database, we found interactions between Sting1 and Tbk1, IRF3, and cGAS in both humans and mice (Figure 4e and f). Next, we will verify the expression of the cGAS-STING pathway in the raw264.7 cell line.

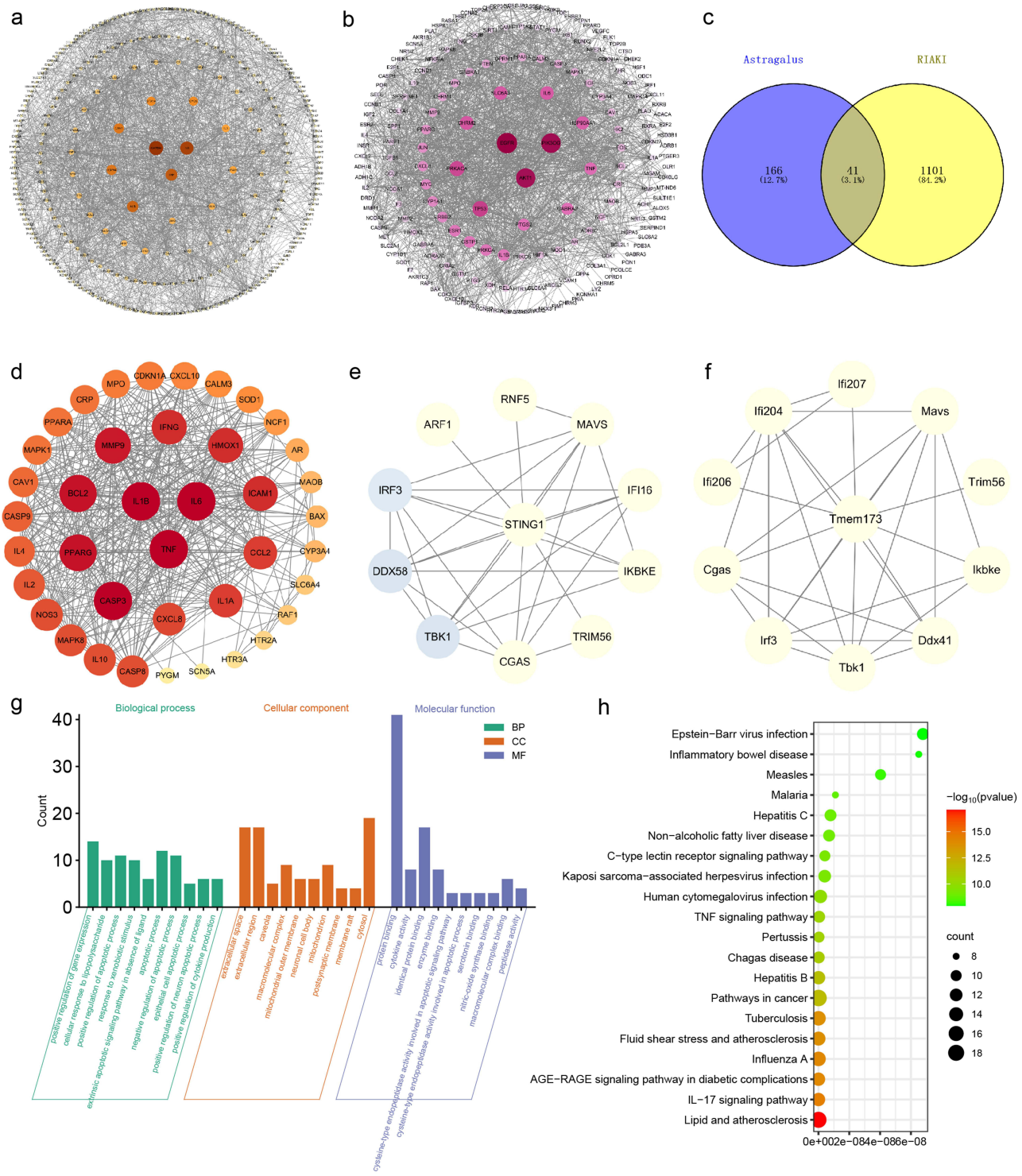

Figure 4 Target Screening of RIAKI and Astragalus. (**a**) Targets of RIAKI. (**b**) Targets of Astragalus. (**c**) Intersection targets of RIAKI and Astragalus. (**d**) PPI network diagram of intersection targets of RIAKI and Astragalus. (**e**) PPI network diagram of human Sting1. (**f**) PPI network diagram of mouse Sting1. (**g**) GO analysis of the intersection genes. (**h**) KEGG analysis of the intersection genes.

APS Restrained LPS and IFN-γ-Induced M1 Polarization in raw264.7 Cells

We employed the CCK8 test principally to appraise the consequence of different concentrations of APS on proliferation of raw264.7 cells over 24 or 48 hours (Figure 5a–c). Following 24 hours of exposure to various APS concentrations, we noticed that raw264.7 cells exhibited marginally enhanced cell proliferation but no discernible change in cell activity. It

was heeded that low concentrations of APS did not exert a significant effect on cell viability, whereas a concentration of 800 μg/mL stimulated cell proliferation when the exposure duration extended to 48 hours. We computed the IC50 of APS to be 46.34μg/mL and selected concentrations of 50μg/mL and 100μg/mL for experimental use. Figure 5d is a summary diagram of our cell experiments. Microscopy revealed changes in cellular morphology, raw264.7 cells treated with LPS and IFN-γ appeared irregular with protrusions, while APS-treated cells were mostly rounded (Figure 5e). Flow cytometry analysis indicated a significant upregulation of the M1 macrophage marker CD86 after induction, which was greatly reduced following APS treatment (Figure 5f and g), corresponding to the qPCR results (Figure 5h and i). Furthermore, ELISA analysis of cell culture supernatants unveiled a notable shrink in the secretion of inflammatory cytokines IL-1β, IL-6, and TNF-α from M1 macrophages upon APS treatment consistent with the qPCR results (Figure 5j–o). Immunofluorescence staining for iNOS corroborated an extraordinary plummet in iNOS expression in APS-treated raw264.7 cells (Figure 5p). Taken together, our findings pinpoint that APS can inhibit macrophage M1 polarization in macrophages.

APS Repressed raw264.7 M1 Polarization via cGAS-STING Pathway

We found that APS can reverse M1 polarization of macrophages in both in vivo and in vitro experiments, and we elucidated the underlying mechanism. Our research focused on the cGAS-STING pathway, currently under investigation for its role in inflammation. Initially, Western blotting revealed that APS suppressed the M1 polarization marker iNOS (Figure 6a), which aligned with our flow cytometry and immunofluorescence results (Figure 5f, g, h, i and p). Consistent

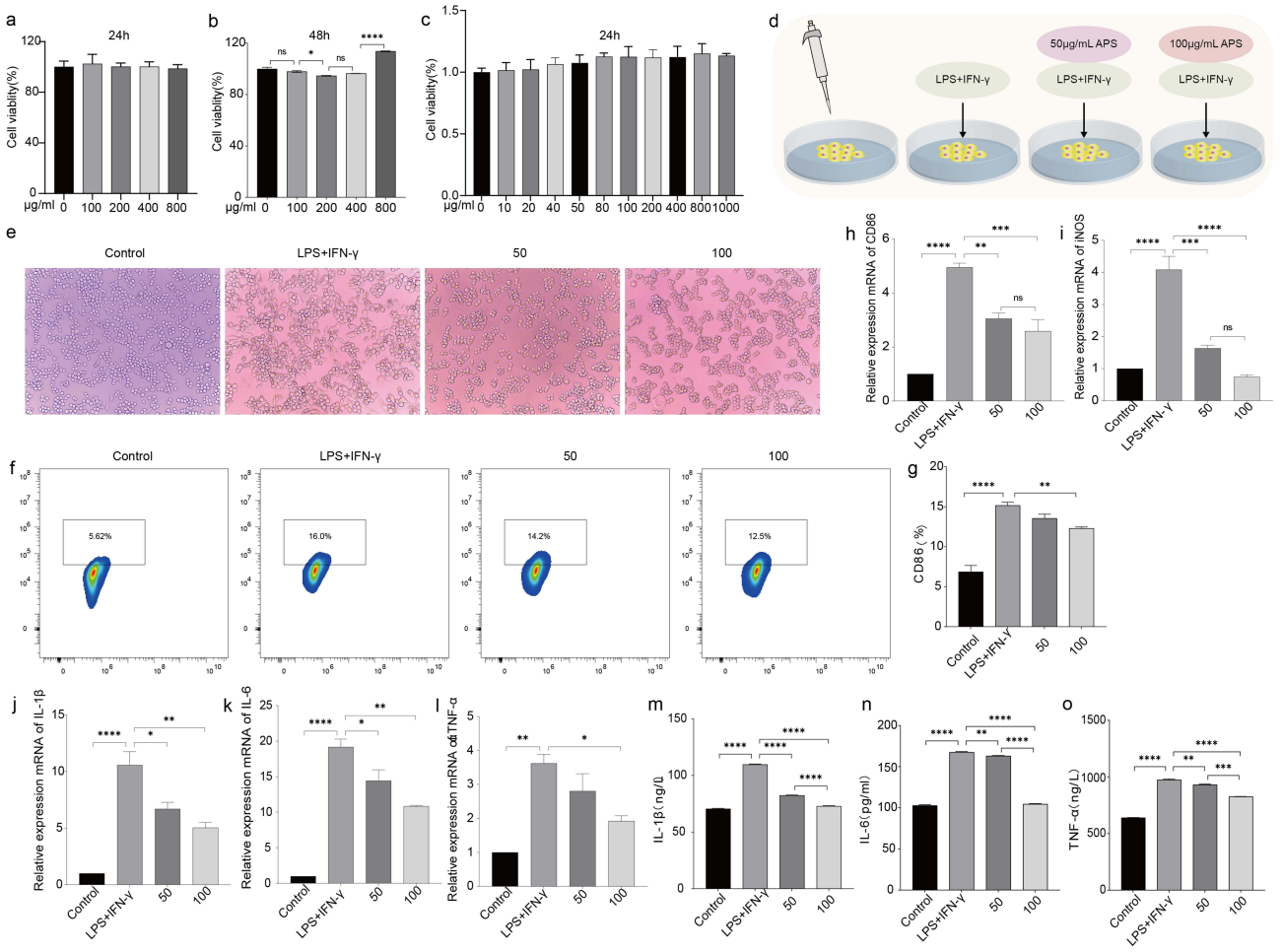

Figure 5 Continued.

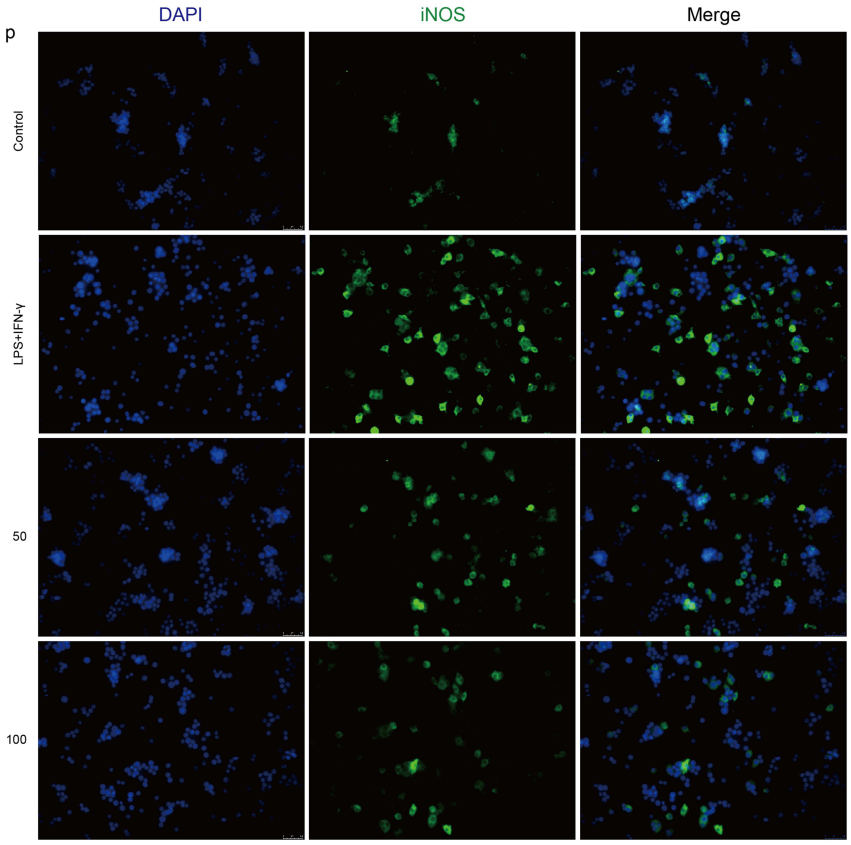

Figure 5 APS restrained LPS and IFN-γ-induced M1 polarization in raw264.7 cells. (**a–c**) Alterations in cell viability of raw264.7 cells appended with distinctive concentrations of APS for 24 or 48 hours. We perceived that when APS was applied to raw264.7 cells for 48 hours, a concentration of 200μg/mL curbed cell viability, whilst a concentration of 800μg/mL triggered cell amplification. When lower concentrations of APS were administered to raw264.7 cells for 24 hours, we inspected a dose-dependent increment in the promotive outcome of APS on the inflation of raw264.7 cells. (**d**) Flowchart of the cell experimental procedure. (**e**) Morphological changes of raw264.7 cells under inconsistent supplement APS for 24 hours. Cells in the control group displayed a rounded shape and clustered growth, while cells in the model group exhibited protrusions and a spindle shape. The spindle-shaped cells of APS adjuvant faded compared to the LPS and IFN-γ group. (**f** and **g**) Flow cytometry and CD86 statistical analysis after inducing raw264.7 into M1 phenotype followed by APS intervention. Results of flow cytometry after induction with 100ng/mL LPS and 20ng/mL IFN-γ followed by APS intervention showed a significant decrease in CD86 expression. (**h–l**) The qPCR analysis of mRNA expression levels of CD86, iNOS, IL-1β, IL-6, and TNF-α. Following APS treatment, there was a significant reduction observed in the expression of M1 macrophage markers CD86 and iNOS, along with a decrement in their secretion of inflammatory cytokines. (**m–o**) Elisa measurement of changes in IL-1β, IL-6, and TNF-α levels in cell culture supernatants. (**p**) Immunofluorescence displaying the expression of iNOS. Control: normal control group; LPS+IFN-γ group: 100ng/mL LPS and 20ng/mL IFN-γ induced raw264.7 M1 polarization model; 50: raw264.7 M1 polarization model with 50μg/mL APS; 100: raw264.7 M1 polarization model with 100μg/mL APS. *p<0.05; **p<0.01; ***p<0.001; ****p<0.0001.
Abbreviation: ns, not statistically significant.

with previous network pharmacology studies, we assessed the expression levels of Sting1 and upstream/downstream markers cGAS and IRF3 using Western blotting and qPCR. These markers were upregulated in the model group but downregulated in all APS-treated groups (Figure 6b–d). Confocal microscopy showed significant nuclear translocation of Sting1 protein in the model group, which decreased following APS treatment (Figure 6e).

To investigate the functional significance of the cGAS-STING axis in RIAKI, we implemented a treatment protocol using the cGAS inhibitor RU.521 (30 μM, R887676, Macklin, China) across different groups. Raw264.7 cells were first stimulated with LPS and IFN-γ for 24 hours to create an M1 polarization model. They were then treated with APS (100μg/mL) or a combination of APS and RU.521 for another 24 hours. We conducted flow cytometric analyses to measure CD86 expression and Western blotting to evaluate cGAS, Sting1, and IRF3 levels. Our results indicated reduced expression of proteins of M1 macrophage marker CD86 (Figure 6f and h), as well as proteins involved in the cGAS-STING signaling pathway—namely, cGAS, Sting1, and IRF3 (Figure 6g, i, j and k). We hypothesized that in the model group, cGAS and Sting1 activation led to gene transcription and subsequent nuclear translocation, which was inhibited

by APS. Based on these findings, we deduced that APS can mitigate M1 polarization by impeding the activation of the cGAS-STING pathway, with enhanced efficacy noted at 100μg/mL.

APS Preserved Kidney Function by Impeding cGAS-STING Pathway in Macrophages

Furthermore, we evaluated the expression levels of renal cGAS-STING pathway proteins by extracting mouse kidney proteins for immunoblotting (Figure 7a–c) and immunohistochemistry of kidney sections (Figure 7d–g), consistent with the kidney qPCR results (Figure 7h–j). We observed elevated protein expression of cGAS, Sting1, and IRF3 in the model group, whereas the pre-treated group exhibited decreased expression. These results indicated that APS awarded renal protective effects in vivo by suppressing the actuation of the renal cGAS-STING pathway.

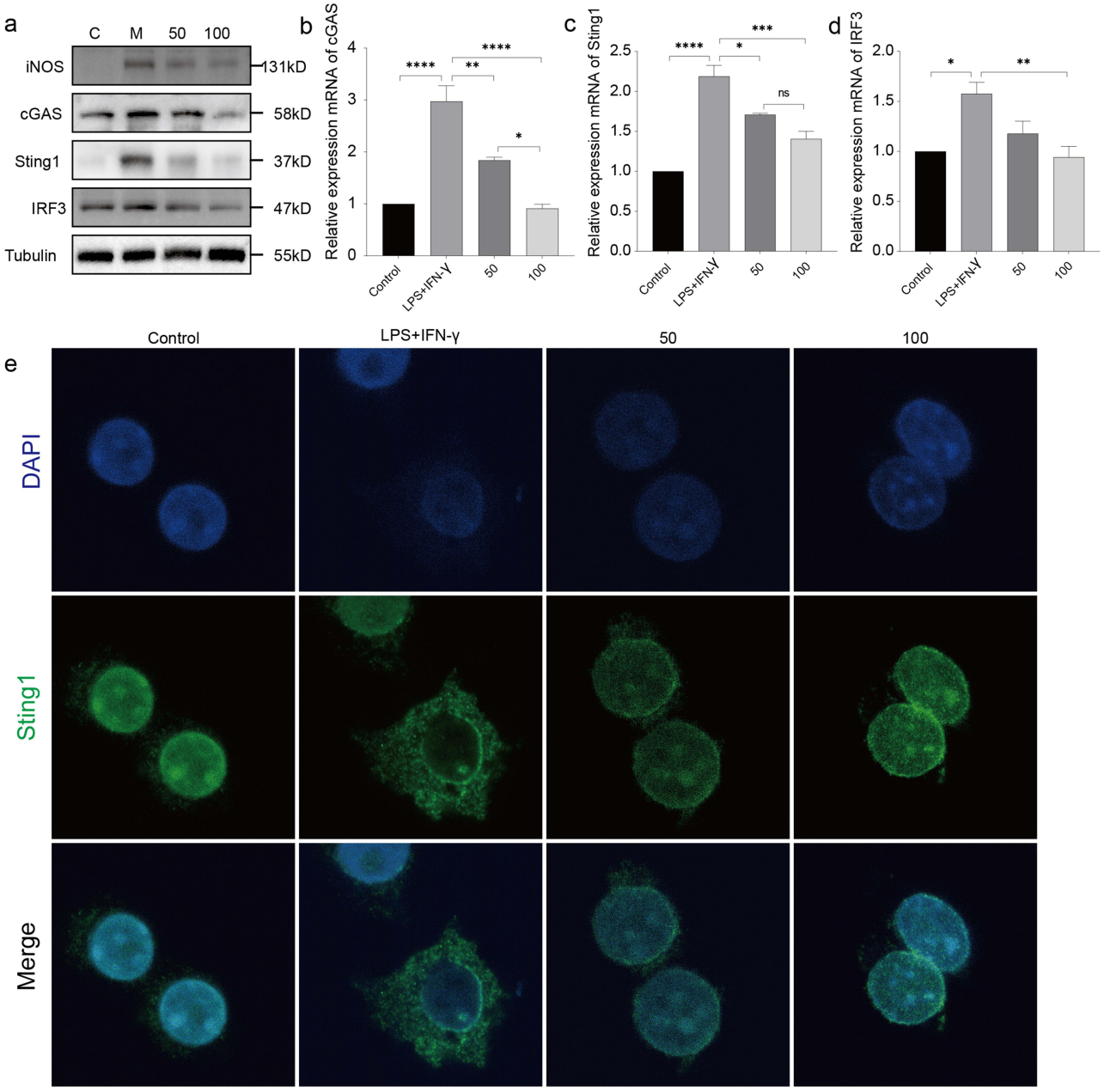

Figure 6 Continued.

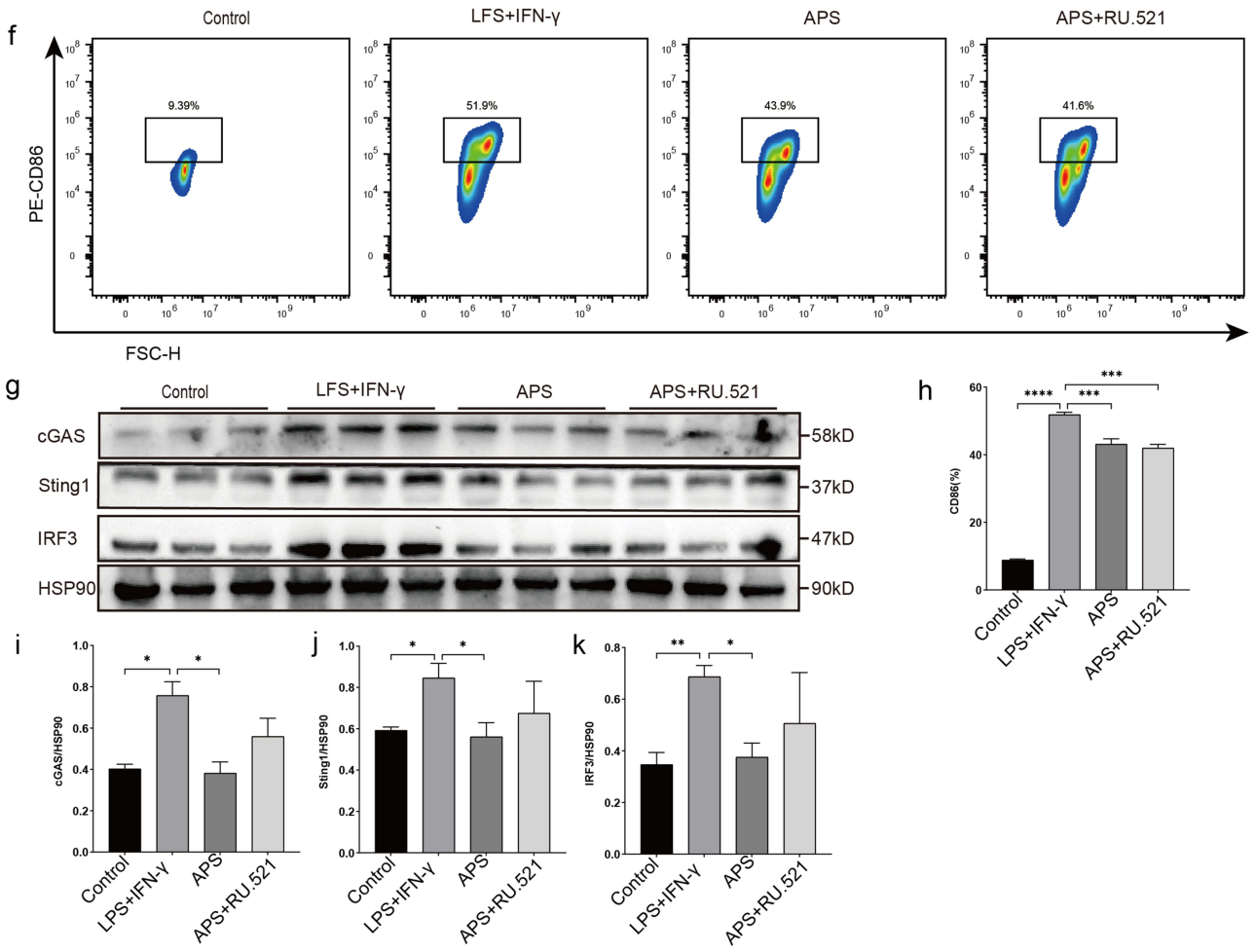

Figure 6 APS repressed raw264.7 M1 polarization via cGAS-STING pathway. (**a**) Western blot bands of protein expression levels of iNOS, cGAS, Sting1, and IRF3 in different groups. (**b–d**) mRNA expression levels of cGAS, Sting1, and IRF3. (**e**) Fluorescent co-localization images of Sting1.Following induction with LPS+IFN-γ, Sting1 translocates prominently from the nucleus, exhibiting magnified expression around the nuclear periphery. Upon APS treatment, its expression predominantly aggregated within the nucleus. This observation propounded that Sting1 expression enriched during the inflammatory process, while APS inhibited Sting1 expression, exerting anti-inflammatory effects. (**f**) We administered APS(100μg/mL) independently and in combination with the cGAS inhibitor RU.521(30μM) to M1 macrophages induced by LPS and IFN-γ. Flow cytometry was employed to quantitatively assess the expression levels of CD86. (**g**) Western blot images depicting the expression levels of cGAS, Sting1, and IRF3. (**h**) The quantification of CD86 expression levels as ascertained through flow cytometric analysis. (**i–k**) Immunoblotting analysis statistical graph of cGAS, Sting1, IRF3. C normal control group; M 100ng/mL LPS and 20ng/mL IFN-γ induced raw264.7 M1 polarization model; 50: raw264.7 M1 polarization model with 50μg/mL APS; 100: raw264.7 M1 polarization model with 100μg/mL APS. *p<0.05; **p<0.01; ***p<0.001; ****p<0.0001.
Abbreviation: ns, not statistically significant.

In in vitro experiments, we discerned that APS possessed the capacity to inhibit the activation of the cGAS-STING signaling axis within macrophages. To further substantiate the activation status of the cGAS-STING pathway in mouse renal macrophages, an immunofluorescence co-staining approach was employed to scrutinize the localization of CD86 and Sting1. Our observations revealed that, in the model group, there was a notable co-localization of CD86 and Sting1 in mouse kidneys (Figure 7k), signifying the activation of Sting1 in M1 macrophages. In contrast, mice that were administered APS exhibited a diminished expression of both CD86 and Sting1 in the renal, which aligned with the findings obtained from in vitro investigations. Consequently, we deduced that in instances of kidney damage precipitated by rhabdomyolysis, the cGAS-STING pathway underwent activation within renal macrophages, leading to a phenotypic switch towards M1 macrophages that predominantly expressed CD86. Notably, APS attenuated the infiltration of renal M1 macrophages by curtailing the activation of the cGAS-STING pathway within these cells, thereby enacting a renoprotective role.

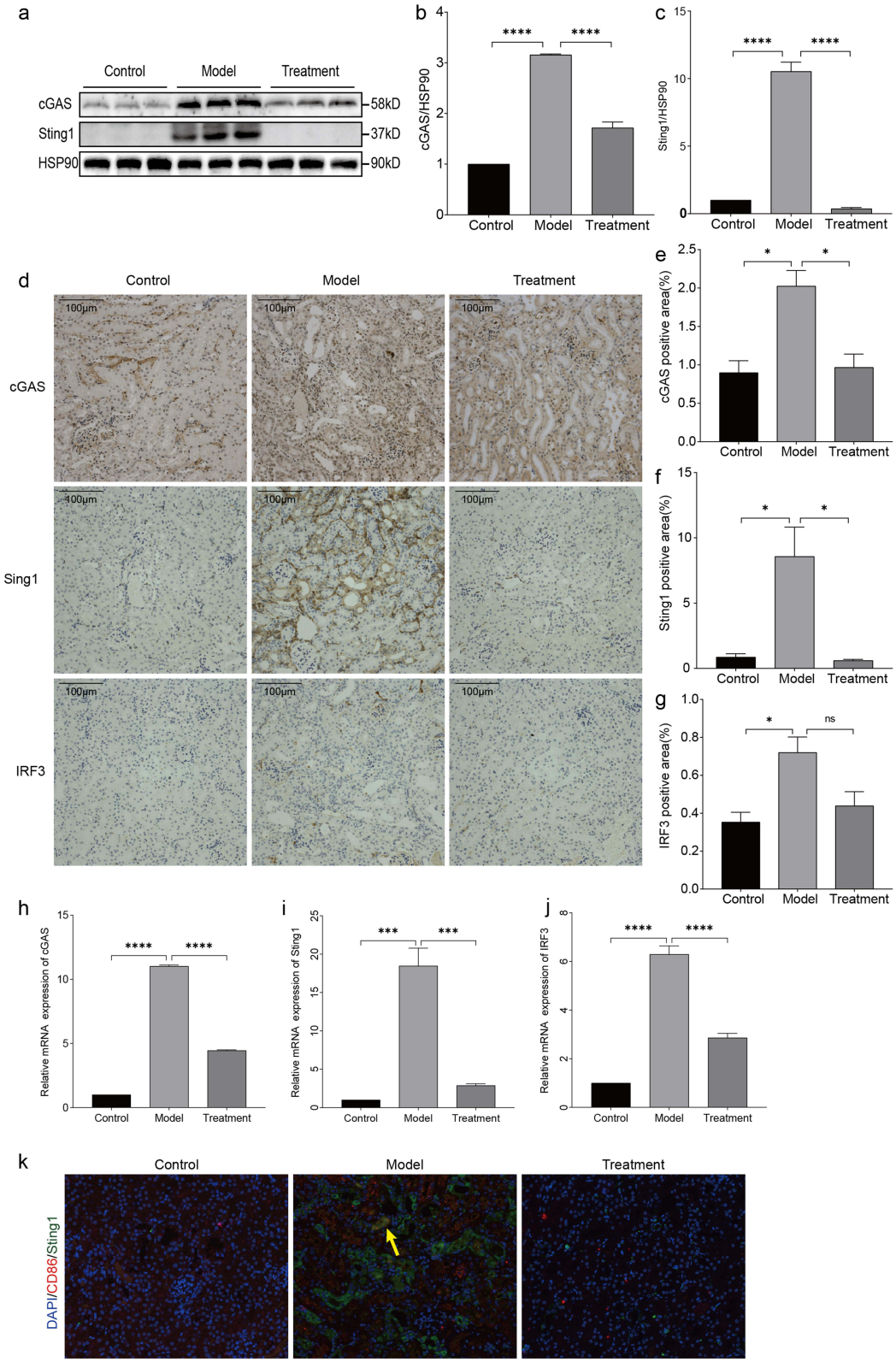

Figure 7 APS preserve kidney function by impeding cGAS-STING pathway in macrophages. (**a–c**) Expression of cGAS and Sting1 proteins in mouse kidneys and statistical graphs of relative expression. (**d–g**) Statistical graphs of relative expression of cGAS, Sting1, and IRF3 proteins in mouse kidneys by immunohistochemistry. (**h–j**) mRNA expression levels of cGAS, Sting1 and IRF3 of kidneys. (**k**) Immunofluorescence co-staining of CD86 (red) and Sting1 (green) of mice kidneys. The yellow arrow indicates the co-localization of CD86 and Sting1, suggesting the activation of Sting1 within M1 macrophages.

Note: *p<0.05; ***p<0.001; ****p<0.0001; Magnification: 20x, scale bar: 100μm.

Abbreviation: ns, no statistical significance.

APS Exerted Renoprotective Effects via Cell Apoptosis Inhibition and Conserving Podocytes

In in vivo and in vitro experiments, we found that M1 macrophages underwent polarization when rhabdomyolysis hit the kidney, and further we assessed BAX/Bcl2, revealing an elevation in renal apoptosis levels (Figure 8a, and d), indicative of increased apoptosis during the progression of RIAKI. Apoptosis is closely consorted with mitochondrial function, thus we conducted markers of mitochondrial function JC1 and reactive oxygen species (ROS) in vitro (Figure 8e and f). In the experimental group, we discovered a thriving in fluorescence intensity, indicative of heightened formation of JC1 monomers along with elevated ROS production (Figure 8e and f). Nonetheless, APS treatment significantly mitigated these effects, demonstrating that APS extenuated macrophage polarization by enhancing mitochondrial function. Acute kidney injury is mainly characterized by tubular injury and necrosis, we found that Nephrin expression was palliated in

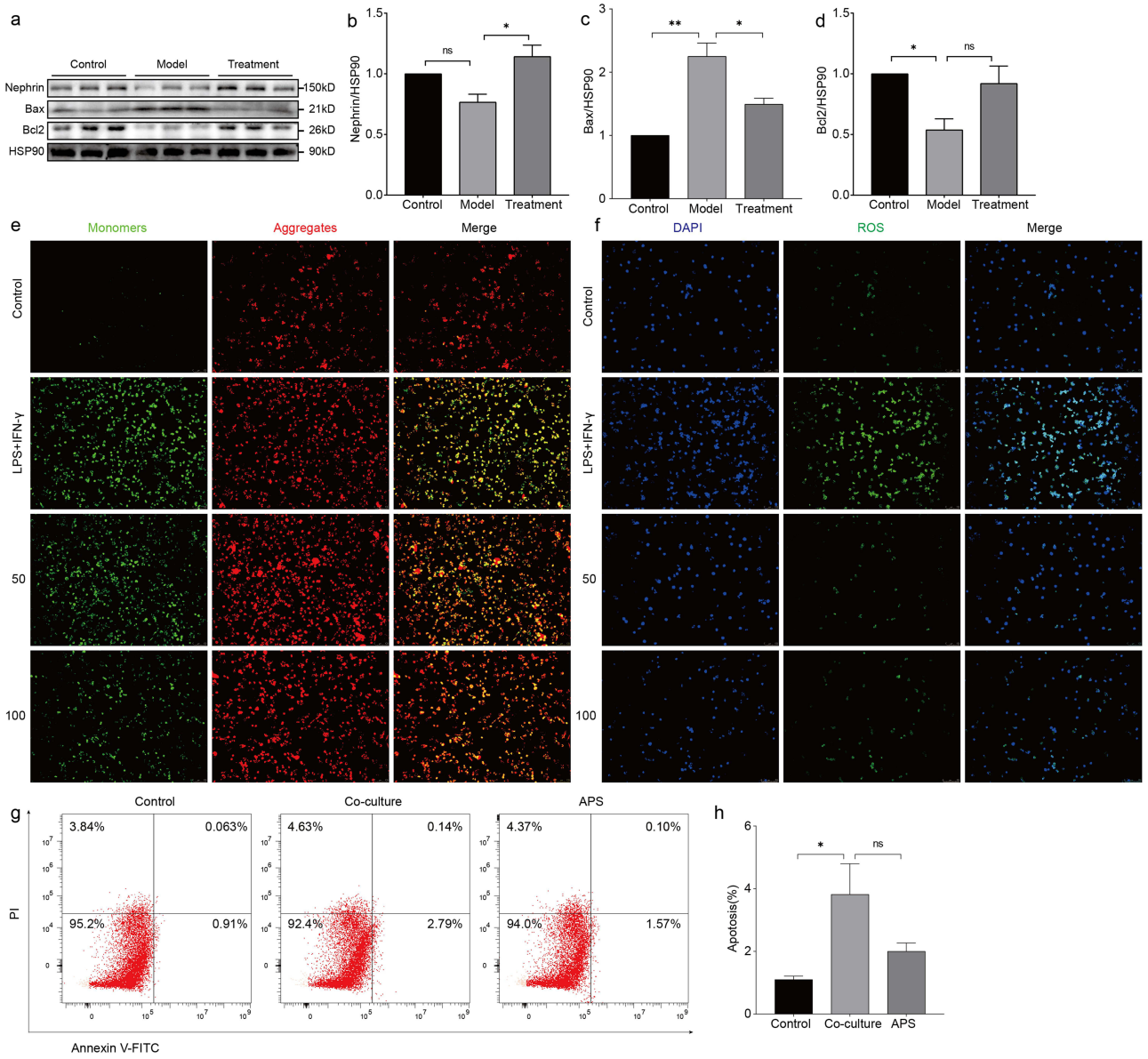

Figure 8 APS exerted renoprotective effects via cell apoptosis inhibition and conserving podocytes. (**a–d**) Immunoblotting bands and statistical graphs depicting Nephrin, Bax, and Bcl2 in mouse kidney tissues. (**e**) Measurement of mitochondrial membrane potential changes by JC-1 in raw264.7 cell lines. (**f**) ROS levels in raw264.7 cell groups. (**g** and **h**) Flow cytometry plots and statistical graphs depicting apoptosis of MPC-5 cells after co-culture with raw264.7 cells. *p<0.05; **p<0.01.
Abbreviation: ns, not statistically significant.

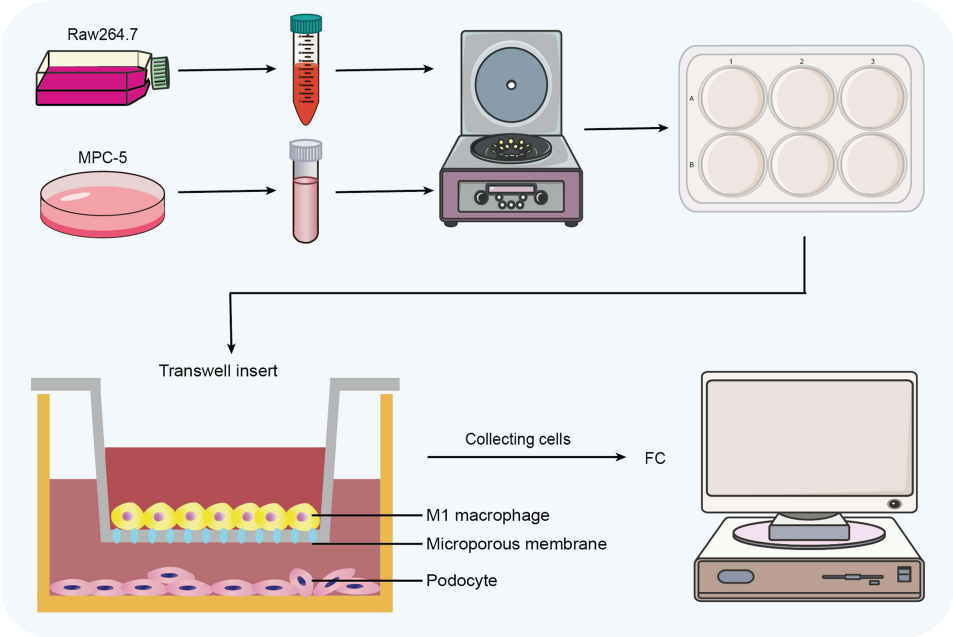

Figure 9 Experimental protocol for co-culture of M1 macrophages and podocytes. We originally induced polarization of raw264.7 cells into M1 macrophages employing a combination of 100 ng/mL LPS and 20 ng/mL IFN-γ. Hereafter, both M1 macrophages and cultured MPC5 cells were harvested. Following centrifugation, MPC5 cells were seeded in a 6-well plate encompassing culture medium supplemented with 100 μg/mL APS. Meanwhile, the M1 macrophages were placed in the upper chamber of a Transwell insert, and following 48 hours of co-culture, the MPC5 cells in the lower chamber were gathered, stained, and subjected to flow cytometric analysis for cell apoptosis.

the mice model group (Figure 8a and b), highlighting the intricate interplay between inflammatory cells and renal cells. We posited that macrophages may interact with podocytes, exacerbating renal injury during acute kidney injury. To explore this hypothesis, we employed transwell chambers in a co-culture system comprising raw264.7 and MPC5 cells to estimate podocyte apoptosis (Figures 8g, 8 and 9). Co-culturing for 48 hours indeed promoted podocyte apoptosis, while APS treatment alleviated podocyte apoptosis. From the foregoing, we concluded that mutual interactions between macrophage polarization and Nephrin expression contribute to podocyte apoptosis over the course of RIAKI, and APS exerted dual protective effects by inhibiting macrophage polarization and safeguarding podocytes, thus offering comprehensive renal protection.

Discussion

Rhabdomyolysis-induced renal injury, a common critical condition in clinical practice, exhibited a fluctuating incidence ranging from 13% to 50%.[1] A single episode of RIAKI accelerated the susceptibility chronic kidney disease (CKD), which contributed to renal ultrastructural abnormalities and a gradual deterioration in renal function that eventually developed into renal fibrosis and CKD.[4–6,25] Renal vasoconstriction, activation of the renin-angiotensin system, decreased effective blood volume, muscular edema, and altered body fluid redistribution were some of the homeostatic mechanisms that occurred during rhabdomyolysis.[1] Following rhabdomyolysis, myoglobin were released from muscle cells, filtered through the bloodstream by the kidneys, and entered cells via endocytosis by megalin-cubilin receptor on the renal tubular epithelium.[26] Intracellularly, ferrous (Fe^{2+}) myoglobin oxidized to trivalent iron (Fe^{3+}), which brought about the production of hydroxyl radicals, lipid peroxidation, depletion of GSH, and mediated protein and DNA damage[27] and renal tubular epithelium underwent oxidative stress, necrosis, apoptosis, and ferroptosis, fostering AKI.[26–31]

Macrophages played a pivotal role in RIAKI. In glycerol-induced rat kidney injury, there were notable accumulation in interstitial macrophage numbers at the early stage, primarily concentrated in the outer medulla, accompanied by momentous apoptotic tubular epithelial cells.[28] On top of that, researchers indicated that predominance of M1 macrophages shortly after glycerol administration, transitioning to a domination of M2 macrophages during the recovery

phase,[5,9–11,32,33] paralleling changes in renal function markers to mention UREA and CREA. Notably, pre-depletion of macrophages with liposomal clodronate minimized the abundance of both M1 and M2 macrophages, restoring renal capability in estimated glomerular filtration rate (eGFR), attenuating of long-term renal fibrosis, and enhancing survival rates. In vitro experiments advocated that myoglobin prompted macrophage polarization towards both M1 and M2 phenotypes,[5,33] denoting a phenotypic transformation of macrophages in the context of RIAKI. Furthermore, following the release of myoglobin and subsequent breakdown of heme into hemoglobin, activated platelets engaged with Mac-1 receptors on macrophages, thereby instigating the generation of reactive oxygen species (ROS), histone citrullination, and the formation of macrophage extracellular traps (MET). Retarding Mac-1 and/or directly targeting MET could potentially prevent platelet-mediated MET formation and RIAKI, while neutrophil depletion appeared ineffective.[34] These findings underscored the paramount role of macrophages in both facilitating renal impairment and bestowing kidney safeguarding benefits in RIAKI. In proximal renal tubules, inhibitors targeting the megalin receptor, such as cilastatin, and cystathionine-γ-lyase-1 antagonists alleviated macrophage infiltration and advanced RIAKI.[2,28] In cisplatin-induced renal injury models, macrophages and inflammatory cytokines such as IL-1β and TNF-α were found to increase on the first day,[28,35] aligning with our research findings.

The cGAS-STING pathway served as a indispensable mechanism within the innate immune system, participating in the regulation of inflammation and energy homeostasis under conditions such as obesity, renal fibrosis, and AKI.[36–40] In the course of RIAKI, escalation in the level of double-stranded DNA (dsDNA) precipitated trauma and irritation in renal epithelial cells. Research highlighted that Aim2 deficiency yielded the accumulation of macrophages, inciting the STING-TBK1-IRF3/NF-κB pathway, thereby spurring the maturation and secretion of pro-inflammatory cytokines, propelling cell pyroptosis, delaying renal function recovery, and exacerbating renal fibrosis. Regimen of DNase-I palliated the immunopathological adjustments mediated by dsDNA in RIAKI. This presumed that dsDNA-induced macrophage pyroptosis may serve as an anti-inflammatory mechanism and dictated the healing process in RIAKI.[6] The evidence from our investigation pointed that in the midst of RIAKI, cGAS-STING pathways were activated in both renal and macrophage, implicating the involvement of inflammatory factor release and recruitment of inflammatory cells to the kidney, cytoplasmic DNA, and mitochondrial DNA damage, which ignited the cGAS-STING pathway, contributing to the development of AKI.[40] However, studies had also shown that STING activation did not count on cGAS,[39] indicating the essentiality for further investigation into the obligations of cGAS and STING in RIAKI.

Both renal interstitial fibrosis and podocyte lesion manifested concurrently in AKI. Research had identified the involvement of the TWEAK/Fn14 axis in kidney injury interconnected with rhabdomyolysis, wherein myoglobin elicited the upregulation of Fn14 both in vivo and in vitro via Nrf2-dependent mechanism, consequently exacerbating renal fibrosis. Genetic deficiency of TWEAK or Fn14 or injection with anti-TWEAK antibodies can optimize renal dysfunction, inflammation, fibrosis, cell death, and oxidative stress, subduing both early and late stages of kidney injury caused by rhabdomyolysis.[30] In murine models of ischemia-reperfusion injury, initial assessments indicated podocyte injury characterized by widespread foot process fusion, accompanied by proteinuria and renal fibrosis.[41,42] Furthermore, onset of STING had been unveiled to motivate albuminuria and podocyte depletion, with genetic or pharmacological prohibition of STING effectively impeding the progression of kidney disease.[38] In LPS-induced pig models of AKI, Masson's staining accentuated the existence of fibrotic elements.[43] Immunostaining studies uncovered the co-localization of α-SMA and the endothelial cell marker CD31 in the tubulointerstitium, conveying an early occurrence of endothelial-to-mesenchymal transition within an hour of model induction.[43] Additionally, a retrospective clinical investigation had documented cases of AKI and proteinuria among patients succumbing to COVID-19 infection, with pathological examination reflecting podocyte effacement, vacuolation, and detachment from the glomerular basement membrane.[44] Integration of our research findings exhibited that reduced podocyte markers Nephrin and increased apoptosis in co-culture with macrophages in RIAKI underscored the simultaneous occurrence of podocyte injury and interstitial fibrosis in early RIAKI. The underlying mechanisms may involve infiltration of inflammatory cells, cytokine storms, vasoconstriction, and renal hypoperfusion, leading to exacerbation of podocyte and renal tubular epithelial cell insults, fostering proteinuria and decreased glomerular filtration rate. This cascade further perpetuated the proceeding of AKI and spured post-injury fibrosis, ultimately culminating in the evolution of chronic kidney disease.[41]

Astragalus membranaceus, a traditional Chinese medicinal herb with a rich history of clinical usage, is employed for the improvement and management of various ailments, serving both medicinal and dietary purposes in invigorating the

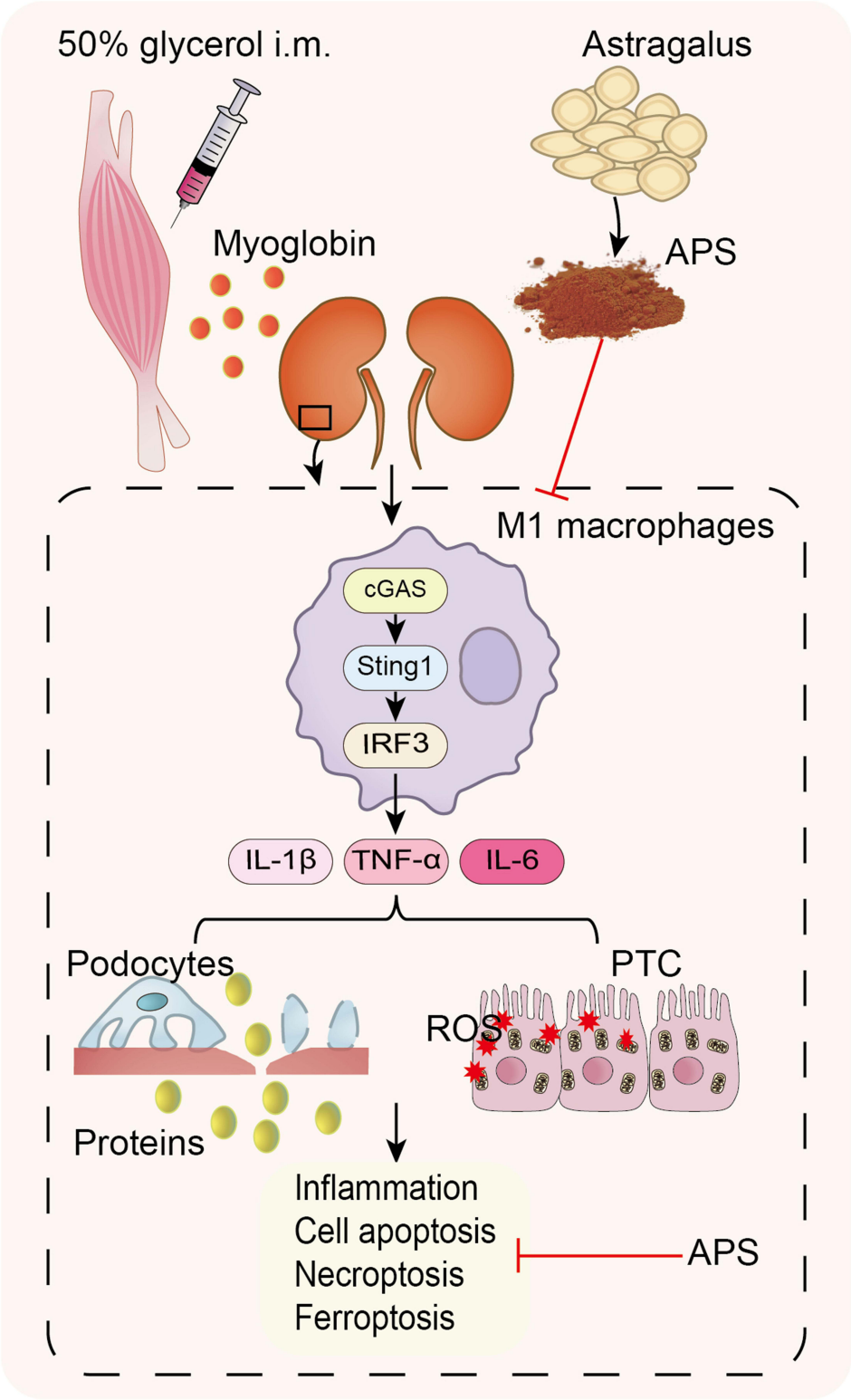

Figure 10 APS alleviates rhabdomyolysis-induced kidney injury mechanisms. Injection of glycerol into muscles induced rhabdomyolysis, triggering the release of enormous myoglobin into the bloodstream. This phenomenon culminated in renal injury and elicited an inflammatory response. Such a response not only compromised the functionality of intrinsic renal cells, including renal tubular epithelial cells and podocytes, thereby prompting programmed cell death pathways such as apoptosis, necrosis, and ferroptosis, but also prompted the activation of renal macrophages towards the M1 phenotype, resulting in the secretion of pro-inflammatory cytokines. Additionally, polarized macrophages were capable of engaging in reciprocal interactions with intrinsic renal cells, further exacerbating renal inflammation. Pretreatment with Astragalus polysaccharide had been shown to mitigate renal oxidative stress and confer protection upon podocytes and renal tubular epithelial cells against injury.
Abbreviations: APS, Astragalus polysaccharide; PTC, Proximal tubule cells; ROS, Reactive oxygen species; →, representative of promotion; ⊣, representative of inhibition.

spleen and replenishing qi. APS is the primary active ingredient extracted from the root of Astragalus membranaceus,[45] which is water-soluble and possesses various pharmacological properties, including immune regulation, anti-aging, anti-tumor, blood sugar regulation, antiviral, anti-fibrotic, lipid-lowering, and antimicrobial effects.[13] APS encompassed polysaccharides such as arabinogalactan, heteropolysaccharides, acidic polysaccharides, and neutral polysaccharides.[46] APS exhibited actions on abundant immune organs, augmenting organ weight, enhancing organ indices, and promoting the development of specific visceral organs. Under varied conditions, APS demonstrates distinct impacts on cytokine production. During normal physiological states, APS can stimulate cytokine production, thereby bolstering immunity. Conversely, amidst inflammatory responses leading to heightened cytokine levels, APS mitigates inflammatory factors and safeguards cells or the organism.[13] APS depreciated intracellular ROS generation, upsurged mitochondrial membrane potential, and preserves mitochondrial morphology, resultantly alleviating cisplatin-induced oxidative damage and mitochondria-mediated apoptosis of renal tubular epithelial cells (TECs) in vitro and in vivo.[47,48] In a rat model of sepsis provoked by cecal ligation and puncture (CLP), APS conveyed pronounced palliative effects, incorporating amelioration of microbiota structure, reduction in levels of pro-inflammatory cytokines such as TNF-α, IL-6, and CRP, mitigation of renal pathological changes distinguished by tubular dilation and congestion, as well as notable attenuation of renal cell apoptosis.[49] By repressing the NF-κB-mediated cytokine pathway, APS curtailed the production of IL-2, IL-6, TNF-α, proficiently deterring glomerulonephritis generated by cationic Bovine Serum Albumin (C-BSA).[50] APS stimulates cytokine production in raw264.7 cells by activating the MAPK and NF-κB signaling pathways mediated by TLR4.[51] Furthermore, APS downregulated ILK expression and curbed the TGF-β/Smad signaling pathway, polishing renal function and minimizing renal fibrosis.[52] APS might protect kidney against STZ-induced injury via increasing the expression of nephrin and podocin in podocytes.[53] Our study findings illustrated that APS can quench ROS, amplify mitochondrial membrane potential, retrench cytokine synthesis, hinder macrophage polarization and kidney deterioration, while concurrently quelling apoptosis and sheltering podocytes in vivo and vitro, possible mechanisms depicted in Figure 10. However, contrary to our observations, some literature intimated that at a concentration of 1000 μg/mL, APS upregulates nitric oxide (NO) and TNF-α to instigate M1 macrophage polarization, correspondingly, encouraging M2 polarization, thus leveraging anti-tumor effects.[54,55] This bidirectional modulation of macrophage polarization by APS may be dosage-dependent, underscoring the criticality of selecting an appropriate APS dosage based on the intended therapeutic outcome.

Our study findings provide novel insights into the prevention and treatment of RIAKI. However, APS primarily absorbed via the gastrointestinal tract after oral administration. The presence of coexisting components in traditional Chinese medicine extracts may influence the pharmacokinetics of the oral drug. Challenges currently include improving its purification process, enhancing drug solubility, inhibiting intestinal metabolism and efflux, and altering the pathways of drug absorption and transportation to promote its bioavailability. Moreover, a single AKI model cannot fully elucidate the therapeutic effects of APS on AKI; therefore, further validation of APS's renoprotective effects in other AKI models is necessary.

Conclusion

In conclusion, the findings of this study underscored the considerable protective efficacy of APS in attenuating RIAKI by suppressing M1 polarization, with underlying mechanism potentially smothering of the cGAS-STING signaling pathway, further decreasing levels of pro-inflammatory cytokines, including TNF-α, IL-1β. These results offered valuable theoretical and practical insights, laying a solid groundwork for the continued investigation and development of APS as a potential therapeutic intervention for acute kidney injury.

Abbreviations

AKI, Acute kidney injury; APS, Astragalus polysaccharide; BSA, Bovine serum albumin; CKD, Chronic kidney disease; CLP, Cecal ligation and puncture; CREA, Serum creatinine; DMEM, Dulbecco's Modified Eagle Medium; eGFR, Estimated glomerular filtration rate; ELISA, Enzyme Linked Immunosorbent Assay; FBS, Foetal bovine serum; GO, Gene Ontology; H&E, Hematoxylin and eosin; IFN-γ, Interferon-γ; KEGG, Kyoto Encyclopedia of Genes and Genomes; LPS, Lipopolysaccharides; MET, Macrophage extracellular traps; MYO, Myoglobin; PAS, Periodic acid Schiff; PPI, Protein–protein interaction; qPCR, Quantitative polymerase-chain reaction; RIAKI, Rhabdomyolysis-induced acute

kidney injury; ROS, Reactive oxygen species; STZ, Streptozotocin; TECs, Tubular epithelial cells; UREA, Blood Urea Nitrogen; WB, Western blotting; KIM-1, kidney injury molecule-1; NGAL, neutrophil gelatinase-associated lipocalin.

Acknowledgments

This study was supported by the Traditional Chinese Medicine Bureau of Guangdong Province (No. 20213005), Administration of Traditional Chinese Medicine of Guangdong Province(No.20232026), Science and Technology Projects in Guangzhou(No.202201010018), Guangdong Provincial Department of Traditional Chinese Medicine Research Project (No. 20221109), and Science and Technology Projects in Guangzhou (No. 2024A03J0832).

Author Contributions

Chuanchuan Sun is the first author. All authors made a significant contribution to the work reported, whether that is in the conception, study design, execution, acquisition of data, analysis and interpretation, or in all these areas; took part in drafting, revising or critically reviewing the article; gave final approval of the version to be published; have agreed on the journal to which the article has been submitted; and agree to be accountable for all aspects of the work.

Disclosure

This paper is available on SSRN as a preprint https://papers.ssrn.com/sol3/papers.cfm?abstract_id=4816453.

The authors declare no conflict of interest.

References

1. Bosch X, Poch E, Grau JM. Rhabdomyolysis and acute kidney injury. *N Engl J Med*. 2009;361(1):62–72. doi:10.1056/NEJMra0801327
2. Matsushita K, Mori K, Saritas T, et al. Cilastatin ameliorates rhabdomyolysis-induced AKI in mice. *J Am Soc Nephrol*. 2021;32(10):2579–2594. doi:10.1681/ASN.2020030263
3. Gupta A, Thorson P, Penmatsa KR, et al. Rhabdomyolysis: revisited. *Ulster Med J*. 2021;90(2):61–69. doi:10.1093/med/9780199592548.001.0001/med-9780199592548-chapter-252
4. Candela N, Silva S, Georges B, et al. Short- and long-term renal outcomes following severe rhabdomyolysis: a French multicenter retrospective study of 387 patients. *Ann Intensive Care*. 2020;10(1):27. doi:10.1186/s13613-020-0645-1
5. Belliere J, Casemayou A, Ducasse L, et al. Specific macrophage subtypes influence the progression of rhabdomyolysis-induced kidney injury. *J Am Soc Nephrol*. 2015;26(6):1363–1377. doi:10.1681/ASN.2014040320
6. Baatarjav C, Komada T, Karasawa T, et al. dsDNA-induced AIM2 pyroptosis halts aberrant inflammation during rhabdomyolysis-induced acute kidney injury. *Cell Death Differ*. 2022;29(12):2487–2502. doi:10.1038/s41418-022-01033-9
7. Petejova N, Martinek A. Acute kidney injury due to rhabdomyolysis and renal replacement therapy: a critical review. *Crit Care*. 2014;18(3):224. doi:10.1186/cc13897
8. Wynn TA, Chawla A, Pollard JW. Macrophage biology in development, homeostasis and disease. *Nature*. 2013;496(7446):445–455. doi:10.1038/nature12034
9. Wang S, Zhang C, Li J, et al. Erythropoietin protects against rhabdomyolysis-induced acute kidney injury by modulating macrophage polarization. *Cell Death Dis*. 2017;8(4):e2725. doi:10.1038/cddis.2017.104
10. Rubio-Navarro A, Carril M, Padro D, et al. CD163-macrophages are involved in rhabdomyolysis-induced kidney injury and may be detected by MRI with targeted gold-coated iron oxide nanoparticles. *Theranostics*. 2016;6(6):896–914. doi:10.7150/thno.14915
11. Rao SN, Zahm M, Casemayou A, et al. Single-cell RNA sequencing identifies senescence as therapeutic target in rhabdomyolysis-induced acute kidney injury. *Nephrol Dial Transplant*. 2024;39(3):496–509. doi:10.1093/ndt/gfad199
12. Hebert JF, Burfeind KG, Malinoski D, et al. Molecular mechanisms of rhabdomyolysis-induced kidney injury: from bench to bedside. *Kidney Int Rep*. 2023;8(1):17–29. doi:10.1016/j.ekir.2022.09.026
13. Zheng Y, Ren W, Zhang L, et al. A review of the pharmacological action of astragalus polysaccharide. *Front Pharmacol*. 2020;11:349. doi:10.3389/fphar.2020.00349
14. Johnson AC, Stahl A, Zager RA. Triglyceride accumulation in injured renal tubular cells: alterations in both synthetic and catabolic pathways. *Kidney Int*. 2005;67(6):2196–2209. doi:10.1111/j.1523-1755.2005.00325.x
15. Boudhabhay I, Poillerat V, Grunenwald A, et al. Complement activation is a crucial driver of acute kidney injury in rhabdomyolysis. *Kidney Int*. 2021;99(3):581–597. doi:10.1016/j.kint.2020.09.033
16. Cheung MD, Erman EN, Moore KH, et al. Resident macrophage subpopulations occupy distinct microenvironments in the kidney. *JCI Insight*. 2022;7(20). doi:10.1172/jci.insight.161078
17. Wei Q, Hill WD, Su Y, et al. Heme oxygenase-1 induction contributes to renoprotection by G-CSF during rhabdomyolysis-associated acute kidney injury. *Am J Physiol Renal Physiol*. 2011;301(1):F162–70. doi:10.1152/ajprenal.00438.2010
18. Safran M, Chalifa-Caspi V, Shmueli O, et al. Human gene-centric databases at the Weizmann Institute of Science: geneCards, UDB, CroW 21 and HORDE. *Nucleic Acids Res*. 2003;31(1):142–146. doi:10.1093/nar/gkg050
19. Amberger JS, Bocchini CA, Schiettecatte F, et al. OMIM.org: online Mendelian inheritance in man (OMIM®), an online catalog of human genes and genetic disorders. *Nucleic Acids Res*. 2014;43(D1):D789–D798. doi:10.1093/nar/gku1205

20. Zhou Y, Zhang Y, Zhao D, et al. TTD: therapeutic target database describing target druggability information. *Nucleic Acids Res*. 2024;52(D1): D1465–d1477. doi:10.1093/nar/gkad751
21. Huang C, Zheng C, Li Y, et al. Systems pharmacology in drug discovery and therapeutic insight for herbal medicines. *Brief Bioinform*. 2014;15 (5):710–733. doi:10.1093/bib/bbt035
22. Bateman A, Martin M-J, Orchard S. UniProt: the universal protein knowledgebase in 2021. *Nucleic Acids Res*. 2021;49(D1):D480–d489. doi:10.1093/nar/gkaa1100
23. Szklarczyk D, Kirsch R, Koutrouli M, et al. The STRING database in 2023: protein-protein association networks and functional enrichment analyses for any sequenced genome of interest. *Nucleic Acids Res*. 2023;51(D1):D638–d646. doi:10.1093/nar/gkac1000
24. Sherman BT, Hao M, Qiu J, et al. DAVID: a web server for functional enrichment analysis and functional annotation of gene lists (2021 update). *Nucleic Acids Res*. 2022;50(W1):W216–w221. doi:10.1093/nar/gkac194
25. Murugan R, Kellum JA. Acute kidney injury: what's the prognosis? *Nat Rev Nephrol*. 2011;7(4):209–217. doi:10.1038/nrneph.2011.13
26. Gburek J, Birn H, Verroust PJ, et al. Renal uptake of myoglobin is mediated by the endocytic receptors megalin and cubilin. *Am J Physiol Renal Physiol*. 2003;285(3):F451–8. doi:10.1152/ajprenal.00062.2003
27. Panizo N, Rubio-Navarro A, Amaro-Villalobos JM, et al. Molecular mechanisms and novel therapeutic approaches to rhabdomyolysis-induced acute kidney injury. *Kidney Blood Press Res*. 2015;40(5):520–532. doi:10.1159/000368528
28. Homsi E, Janino P, de Faria JBL. Role of caspases on cell death, inflammation, and cell cycle in glycerol-induced acute renal failure. *Kidney Int*. 2006;69(8):1385–1392. doi:10.1038/sj.ki.5000315
29. Guerrero-Hue M, García-Caballero C, Palomino-Antolín A, et al. Curcumin reduces renal damage associated with rhabdomyolysis by decreasing ferroptosis-mediated cell death. *FASEB j*. 2019;33(8):8961–8975. doi:10.1096/fj.201900077R
30. Guerrero-Hue M, Vallejo-Mudarra M, García-Caballero C, et al. Tweak/Fn14 system is involved in rhabdomyolysis-induced acute kidney injury. *Biomed Pharmacother*. 2023;169:115925. doi:10.1016/j.biopha.2023.115925
31. Kumar S. Cellular and molecular pathways of renal repair after acute kidney injury. *Kidney Int*. 2018;93(1):27–40. doi:10.1016/j.kint.2017.07.030
32. Sinniah R, Lye W. Acute renal failure from myoglobinuria secondary to myositis from severe falciparum malaria. *Am J Nephrol*. 2000;20(4):339–343. doi:10.1159/000013611
33. Madsen DH, Leonard D, Masedunskas A, et al. M2-like macrophages are responsible for collagen degradation through a mannose receptor-mediated pathway. *J Cell Biol*. 2013;202(6):951–966. doi:10.1083/jcb.201301081
34. Okubo K, Kurosawa M, Kamiya M, et al. Macrophage extracellular trap formation promoted by platelet activation is a key mediator of rhabdomyolysis-induced acute kidney injury. *Nat Med*. 2018;24(2):232–238. doi:10.1038/nm.4462
35. Nozaki Y, Kinoshita K, Yano T, et al. Signaling through the interleukin-18 receptor α attenuates inflammation in cisplatin-induced acute kidney injury. *Kidney Int*. 2012;82(8):892–902. doi:10.1038/ki.2012.226
36. Gulen MF, Samson N, Keller A, et al. cGAS-STING drives ageing-related inflammation and neurodegeneration. *Nature*. 2023;620(7973):374–380. doi:10.1038/s41586-023-06373-1
37. Motwani M, Pesiridis S, Fitzgerald KA. DNA sensing by the cGAS-STING pathway in health and disease. *Nat Rev Genet*. 2019;20(11):657–674. doi:10.1038/s41576-019-0151-1
38. Mitrofanova A, Fontanella A, Tolerico M, et al. Activation of stimulator of IFN genes (STING) causes proteinuria and contributes to glomerular diseases. *J Am Soc Nephrol*. 2022;33(12):2153–2173. doi:10.1681/ASN.2021101286
39. Long Y, Guo J, Chen J, et al. GPR162 activates STING dependent DNA damage pathway as a novel tumor suppressor and radiation sensitizer. *Signal Transduct Target Ther*. 2023;8(1):48. doi:10.1038/s41392-022-01224-3
40. Sun C, Shi H, Zhao X, et al. The activation of cGAS-STING in acute kidney injury. *J Inflamm Res*. 2023;16:4461–4470. doi:10.2147/JIR.S423232
41. Chen Y, Lin L, Tao X, et al. The role of podocyte damage in the etiology of ischemia-reperfusion acute kidney injury and post-injury fibrosis. *BMC Nephrol*. 2019;20(1):106. doi:10.1186/s12882-019-1298-x
42. Yu H, Lin T, Chen W, et al. Size and temporal-dependent efficacy of oltipraz-loaded PLGA nanoparticles for treatment of acute kidney injury and fibrosis. *Biomaterials*. 2019;219:119368. doi:10.1016/j.biomaterials.2019.119368
43. Castellano G, Stasi A, Intini A, et al. Endothelial dysfunction and renal fibrosis in endotoxemia-induced oliguric kidney injury: possible role of LPS-binding protein. *Crit Care*. 2014;18(5):520. doi:10.1186/s13054-014-0520-2
44. Su H, Yang M, Wan C, et al. Renal histopathological analysis of 26 postmortem findings of patients with COVID-19 in China. *Kidney Int*. 2020;98 (1):219–227. doi:10.1016/j.kint.2020.04.003
45. Chen Z, Liu L, Gao C, et al. Astragali Radix (Huangqi): a promising edible immunomodulatory herbal medicine. *J Ethnopharmacol*. 2020;258:112895. doi:10.1016/j.jep.2020.112895
46. Shi Y, Shi X, Zhao M, et al. Pharmacological potential of Astragali Radix for the treatment of kidney diseases. *Phytomedicine*. 2024;123:155196. doi:10.1016/j.phymed.2023.155196
47. Ma Q, Xu Y, Tang L, et al. Astragalus polysaccharide attenuates cisplatin-induced acute kidney injury by suppressing oxidative damage and mitochondrial dysfunction. *Biomed Res Int*. 2020;2020:2851349. doi:10.1155/2020/2851349
48. Huang F, Sun X-Y, Chen X-W, et al. Effects of selenized astragalus polysaccharide on the adhesion and endocytosis of nanocalcium oxalate dihydrate after the repair of damaged HK-2 cells. *ACS Biomater Sci Eng*. 2021;7(2):739–751. doi:10.1021/acsbiomaterials.0c01318
49. Li J, Zhao J, Chai Y, et al. Astragalus polysaccharide protects sepsis model rats after cecum ligation and puncture. *Front Bioeng Biotechnol*. 2022;10:1020300. doi:10.3389/fbioe.2022.1020300
50. Li S, Zhang Y, Zhao J. Preparation and suppressive effect of astragalus polysaccharide in glomerulonephritis rats. *Int Immunopharmacol*. 2007;7 (1):23–28. doi:10.1016/j.intimp.2006.08.016
51. Dong M, Li J, Yang D, et al. Biosynthesis and pharmacological activities of flavonoids, triterpene saponins and polysaccharides derived from astragalus membranaceus. *Molecules*. 2023;28(13):5018. doi:10.3390/molecules28135018
52. Zheng W, Huang T, Tang Q-Z, et al. Astragalus polysaccharide reduces blood pressure, renal damage, and dysfunction through the TGF-β1-ILK Pathway. *Front Pharmacol*. 2021;12:706617. doi:10.3389/fphar.2021.706617
53. Yan Z. Effect of astragalus polysaccharin on expression of nephrin and podocin in podocytes of early diabetic nephropathy rats. *Chinese J Pathophysiol*. 2011.

54. Li W, Song K, Wang S, et al. Anti-tumor potential of astragalus polysaccharides on breast cancer cell line mediated by macrophage activation. *Mater Sci Eng*. 2019;98:685–695. doi:10.1016/j.msec.2019.01.025
55. Bamodu OA, Kuo K-T, Wang C-H, et al. Astragalus polysaccharides (PG2) enhances the M1 polarization of macrophages, functional maturation of dendritic cells, and T cell-mediated anticancer immune responses in patients with lung cancer. *Nutrients*. 2019;11(10):2264. doi:10.3390/nu11102264